# The Influence of Sea-ice Parameterizations on the Modelling of Snowball Earth Initiation

Master Thesis in Meteorology
by

**Johannes Hörner**

August 2020


INSTITUTE FOR METEOROLOGY AND CLIMATE RESEARCH
KARLSRUHE INSTITUTE OF TECHNOLOGY (KIT)

| | |
|---|---|
| Advisor: | Dr. Aiko Voigt |
| Second Advisor: | Prof. Dr. Joaquim Pinto |

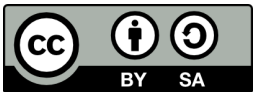

# Abstract

Snowball Earth is a hypothesized state in the deep past of Earth, in which the ocean was completely covered by sea ice. Sea ice is thus a central aspect of the climate dynamics of a Snowball Earth, as it governs the ice-albedo feedback that is responsible for the existence of the Snowball Earth bifurcation. An appropriate representation of sea ice in the modelling of a Snowball Earth is therefore of major importance.
The goal of this work is to investigate how the initiation of a Snowball Earth is influenced by

1. limiting maximum sea-ice thickness to 5 m,

2. different vertical resolutions of the sea-ice scheme.

Three sets of simulations are performed using ICON-AES in an aqua planet setup. The sea-ice schemes used for each are a 0-layer Semtner model with a thickness limit, an unlimited 0-layer Semtner model and a 3-layer reformulated Winton model. Additionally, these sea-ice schemes are investigated in offline Python simulations with idealized atmospheric boundary conditions.
Limiting the thickness of sea-ice results in an artificial heat flux into the atmosphere, because only a thin sea-ice cover separates the relatively warm ocean from the cold atmosphere. The atmospheric $CO_2$ content at which Snowball Earth initiation occurs is therefore reduced by 5%. Increasing the vertical resolution of sea ice introduces a heat capacity, which dampens the the diurnal cycle of surface temperature, decreases surface melting and increases surface albedo. The draw-down of atmospheric $CO_2$ content required for Snowball Earth initiation to occur is reduced. The atmospheric $CO_2$ content at which Snowball Earth initiation occurs is thus increased by 50% in the 3-layer Winton model compared to the 0-layer Semtner model.
Overall, these results show that while the sea-ice thickness limit plays only a minor role, a sufficiently high vertical resolution of sea-ice schemes is important for a realistic representation of Snowball Earth initiation.

# Zusammenfassung

Die Schneeballerde ist ein vermuteter Zustand in der früheren Erdgeschichte, in dem der Ozean komplett vereist war. Meereis ist ein zentraler Aspekt der Schneeballerde, da es das Eis-Albedo-Feedback bestimmt, das für die Bifurkation der Schneeballerde verantwortlich ist. Eine angemessene Repräsentation von Meereis bei Simulationen der Schneeballerde ist dementsprechend von großer Bedeutung.
In dieser Arbeit wird untersucht, wie die Initiierung der Schneeballerde beeinflusst wird von

1. einer Meereisdickenbegrenzung von 5 m,

2. unterschiedlichen vertikalen Auflösungen des Meereisschemas.

Drei Gruppen von Simulationen werden mit ICON-AES in einem Aquaplanetensetup durchgeführt. Die Meereisschemata für die jeweiligen Gruppen sind ein 0-Schichten Semtner Modell mit Meereisdickenbegrenzung, ein unbegrenztes 0-Schichten Semtner Modell und ein 3-Schichten Winton Modell. Zusätzlich werden diese Meereisschemata anhand einer offline Python Simulation mit idealisierten atmosphärischen Randbedingungen untersucht.
Die Meereisdickenbegrenzung führt zu einem künstlichen Hitzefluss in die Atmosphäre, da der verhältnismäßig warme Ozean nur durch eine dünne Eisschicht von der kalten Atmosphäre getrennt ist. Dadurch verringert sich der für die Initiierung der Schneeballerde benötigte $CO_2$ Gehalt um 5%. Das Erhöhen der vertikalen Auflösung des Meereisschemas fügt dem Eis eine Wärmekapazität hinzu. Dadurch wird der tägliche Zyklus der Oberflächentemperaturen gedämpft, was Schmelzen an der Oberfläche verringert und die Oberflächenalbedo erhöht. Die Reduktion des atmosphärischen $CO_2$ Gehalts, die für die Initiierung der Schneeballerde nötig ist, wird dadurch verringert. Der atmosphärische $CO_2$ Gehalt, bei dem eine Initiierung der Schneeballerde eintreten kann, wird daher um 50% erhöht.
Insgesamt zeigen diese Ergebnisse, dass, während die Meereisdickenbegrenzung nur eine untergeordnete Rolle spielt, eine ausreichend hohe vertikale Auflösung des Meereisschemas wichtig für eine realistische Repräsentation der Initiierung der Schneeballerde ist.

# Contents

# 1 Introduction

During the Neoproterozoic, the geological era from 1000 Ma to 541 Ma ago, Earth was subject to multiple global or nearly global glaciation (Pierrehumbert et al., 2011). These pan-glaciations were different than the glaciations in the more recent history of Earth, as the ice cover did not only reach to the mid-latitudes, but the Earth was almost completely covered by ice (Hoffman, 2009). This so called Snowball Earth was arguably one of the most extreme climatic states ever present on Earth, posing an enormous challenge for the survival of early multicellular life in the ocean (Runnegar, 2000). The characteristics of a Snowball Earth are therefore important for the understanding of how life on Earth developed.

The basic mechanism of the initiation of such a Snowball Earth, the ice-albedo feedback, is well known: the brighter ice reflects a larger fraction of the incoming solar radiation, cooling down global temperatures and leading to the further growth of ice (Kirschvink, 1992). When the ice cover reaches a certain latitude, a tipping point is reached and a runaway ice-albedo feedback kicks in. This results in mutually enhancing ice growth and falling temperatures, until global glaciation is achieved. The same effect can lead to the termination of Snowball Earth as well. If ice starts to melt at the equator due to an increasing amount of greenhouse gases in the atmosphere, the runaway ice-albedo feedback takes place in the opposite direction.

However, the characteristics of the bifurcations associated with the initiation of a Snowball Earth still remains a subject of debate. There are various theories on how Earth actually looked like during this time period. Besides the theory of a hard Snowball Earth, where the whole Earth is covered in ice, there are also theories for Waterbelt states or a soft Snowball Earth, where open ocean still is present to some degree (Pierrehumbert et al., 2011). The validity of these theories is strongly related to the representation of various physical effects in simulations of the Neoproterozoic climate. Ice dynamics or a higher ice albedo for example enhance the initiation of a hard Snowball Earth (Yang et al., 2012), whereas ocean currents or cloud radiative forcing inhibit it (Poulsen and Jacob, 2004). The challenge of understanding the characteristics of a Snowball Earth lies therefore in assessing the factors that influence the initiation, termination and stability of Snowball Earth states and in representing these factors in climate models in an appropriate way.

One of these factors are the thermodynamic sea-ice parameterizations that govern the calculation of sea-ice physics. These parameterizations determine the growth and melting of sea ice, as well as the sea-ice surface albedo. An appropriate representation of these processes is important, because they can potentially have a large impact on the sea-ice cover and therefore on the climate of a Snowball Earth. Abbot et al. (2010) showed that using a sea-ice scheme with too few vertical layers hugely overestimates the diurnal temperature cycle by reducing the heat capacity of the sea ice, resulting in increased surface melting and subsequently enhanced Snowball Earth termination. This thesis extends these findings by investigating the influence of vertical resolution of sea-ice schemes on the initiation of Snowball Earth using the ICON general circulation model.

Additionally, the influence of a limited sea-ice thickness on the initiation of Snowball Earth is investigated.
The structure of this thesis is as follows. Chapter 2 gives an overview of the state of the art in the research on Snowball Earth. Chapter 3 then formulates the research questions that are to be answered in this thesis. Chapter 4 describes the sea-ice schemes used in the investigations, as well as the ICON model set-up and further methods. The results of the impact of a limited sea-ice thickness are presented in Chapter 5. Chapter 6 then provides the results of the impact of increased vertical resolution. Ultimately, the conclusion and outlook of this work is given in Chapter 7.

# 2 State of the Art

This chapter provides an overview of the current state of research on Snowball Earth. First, the theory of Snowball Earth and the geological evidence backing it up is described in Section 2.1. Following, a theoretical model is applied to explain the details of the Snowball Bifurcation in Section Section 2.2. Finally, physical effects influencing simulations of Snowball Earth are illustrated in Section 2.3.

## 2.1 The Neoproterozoic Snowball Earth

The basis for the theory of Snowball Earth is provided by various geological data, which gives information about the climate during the Neoproterozoic more than 500 M a ago.
Glacigenic deposits found on multiple continents show the existence of glaciers (Hoffman et al., 2017). Using geochronologic investigations, these proxies can be dated back to two time periods in the Neoproterozoic, the Marinoan 700 M a ago and the Sturtian 635 M a ago. As the positions of continents have been extremely different at this time, there seems to be a vast amount of glacigenic deposits created near the equator (Figure 2.1). Some of these glaciers near the equator even existed at sea level (Hoffman et al., 2017), which indicates a climate that is vastly colder than today's.
Additional proxies are banded iron formations at the ocean floor (Hoffman, 2009). These formations can arise in anoxic ocean water, i.e., ocean water without dissolved oxygen, and they originate from the same time period as the glacigenic deposits. This indicates an ocean that is mostly isolated from the atmosphere, which can be explained by a large scale sea-ice cover.

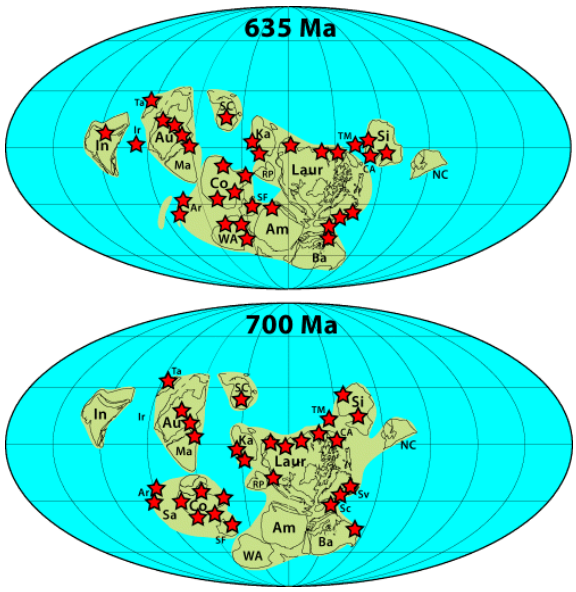


Figure 2.1: Position of glacigenic deposits as red stars dated back to 635 M a (Marinoan) and 700 M a (Sturtian). Figure taken from Hoffman (2009).

Lastly, investigations of cap carbonates dated back to the same time period show a rapid increase of $CO_2$ dissolved in the ocean. This indicates an extremely high atmospheric $CO_2$ content after the global glaciation has ended (Pierrehumbert et al., 2011).
These unusual geological proxies, glacigenic deposits, banded iron formations and cap carbonates, can be explained by a global glaciation. Kirschvink (1992) was the first to postulate such a Neoproterozoic "Snowball Earth" as the origin of the geological evidence.

### Life Cycle of a Snowball Earth

A Snowball Earth starts with the growing of ice sheets and glaciers. The low solar luminosity during the Neoproterozoic, 95% of today's value (Pierrehumbert et al., 2011), facilitates this growth. Additionally, a low atmospheric $CO_2$ content due to efficient silicate weathering caused by the breakup of continents may enhance this (Donnadieu et al., 2004). With the Earth cooling and polar ice sheets and glaciers growing, the planetary albedo is increasing, which results in more sunlight being reflected away from the Earth and global temperatures dropping. The further the ice sheets extend towards the equator into regions with higher solar irradiance, the stronger this effect is. Ultimately, this can lead to a runaway ice-albedo feedback of mutually enhancing ice growth and temperature decrease, which continues until global glaciation is reached. The Earth is now completely covered in ice and snow, and global surface temperatures are far below the freezing point. This explains the glacigenic deposits close to the equator as well as the banded iron formations.
Temperatures have to increase significantly for deglaciation to occur. Volcanic activity leads to outgasing of $CO_2$ and other greenhouse gases into the atmosphere (Pierrehumbert et al., 2011). As the ocean is mostly covered in ice and plants don't exist yet, there exists no major sink of $CO_2$. Thus, atmospheric $CO_2$ is able to reach extremely high values (up to $\sim 10\%$ atmospheric molar concentration, Pierrehumbert et al. (2011)) over the course of multiple million years. This results in temperatures high enough for deglaciation to start at the equator. With the ice starting to melt and bright ice surfaces being replaced by darker ocean surfaces, the runaway ice-albedo feedback takes place in the other direction. Mutually enhancing ice retreat and temperature increase leads to complete melting of the ice cover. Atmospheric $CO_2$ content is still at high levels at this point, resulting in a postglacial hothouse climate. This climate is responsible for the formation of the characteristic cap carbonates.

### The Survival of Life

An arising question is how life in the ocean has been able to survive a Snowball Earth. A thick ice layer on the ocean blocks light from reaching the water, rendering the survival of photosynthetic life in the ocean impossible (Runnegar, 2000). There are multiple theories how photosynthetic life was able to survive such an extreme period in Earth's history. A thin and clear ice cover in the tropics could allow for light to penetrate into the ocean (Warren et al., 2002). Alternatively, life could survive in patches of ice-free water near islands with volcanic activity (Schrag and Hoffman, 2001). Another possibility are waterbelt states: In a Jormungand state, an ice-free strip of open water exists in the tropics, stabilized by the Hadley Cell (Abbot et al., 2011). In this state, ice near the equator is not covered by snow due to being in a region with net surface ablation because of the

descending branch of the Hadley circulation. This results in a lower ice albedo, which ultimately stops the runaway ice-albedo feedback. The existence of a Jormungand state and the transitions between the different climate states can be shown using a theoretical energy balance model. For this, the Budyko-Sellers model is applied in the following section.

## 2.2 Budyko-Sellers - a Theoretical Model

The one dimensional energy balance model developed by Budyko (1969) and Sellers (1969) provides a theoretical framework to explain the existence of the radically different climate states of Earth and the transition between each of these. Following Abbot et al. (2011), the model considers the balance of incoming solar radiation and outgoing longwave radiation with the addition of meridional heat transport, all dependent on latitude:

$$\frac{Q}{4}S(x)\,(1-\alpha(T(x))) = A + BT(x) + C(T(x)-\overline{T}). \tag{2.1}$$

$x = \sin\phi, x \in [0,1]$ is the sine of the latitude $\phi$, assuming symmetry with respect to the equator. The absorbed solar radiation is modeled by the solar constant $Q$, its meridional distribution $S(x)$ and the planetary albedo $\alpha$. $\alpha$ is a function of surface temperature at each latitude. The outgoing longwave radiation is parameterized by a linear function of surface temperature $A + BT(x)$. The impact of the radiative forcing of well-mixed greenhouse gases is considered by variation of the parameter $A$. $B$ is a constant which is chosen to be $B = 1.5\,\mathrm{W\,m^{-2}\,K^{-1}}$. $C(T(x)-\overline{T})$ describes the meridional heat transport depending on the difference between the local temperature at each latitude and global mean temperature.

The meridional distribution of incoming solar radiation $S(x)$ is approximated by:

$$S(x) = 1 - \frac{s_2}{2} + \frac{3}{2}s_2x^2. \tag{2.2}$$

The albedo $\alpha(T(x))$ varies between a lower value $\alpha_1$ for ice-free ocean and clouds, and a higher value $\alpha_2$ for ice-covered ocean, snow and clouds. The ice-free ocean albedo $\alpha_1$ is determined by the albedo of clouds on top of the ocean, whereas the ice-covered ocean albedo $\alpha_2$ is largely determined by the high surface albedo of snow.

$$\alpha(T(x)) = \begin{cases} \alpha_1 & T > T_S \\ \alpha_s = \frac{\alpha_1+\alpha_2}{2} & T = T_S \\ \alpha_2 & T < T_S \end{cases}. \tag{2.3}$$

$T_S$ is the temperature at the ice latitude, i.e., the temperature at which ice forms.

The planetary albedo $\alpha_p(x_s)$, consisting of the ice-free albedo up to the ice latitude and the ice-covered albedo for the rest of the Earth, can be calculated as a function of the latitude of the ice edge $x_s$:

$$\alpha_p(x_s) = \alpha_1 \int_0^{x_s} S(x)\,\mathrm{d}x + \alpha_2 \int_{x_s}^{1} S(x)\,\mathrm{d}x. \tag{2.4}$$

Then the global mean energy balance is calculated by integrating Equation 2.1 over the whole Earth from $x = 0$ to $x = 1$:

$$\frac{Q}{4}(1-\alpha_p(x_s)) = A + B\overline{T}. \tag{2.5}$$

The energy balance from Equation 2.1 at the ice latitude $x = x_S$ results in:

$$\frac{Q}{4}S(x_S)(1-\alpha_S) = A + BT_S + C(T_S - \overline{T}). \tag{2.6}$$

The global mean temperature $\overline{T}$ from Equation 2.6 is then substituted into the global energy balance in Equation 2.5. This can be solved for the radiative forcing $A$ depending on the ice latitude $x_S$:

$$A(x_S) = \frac{1}{1+\frac{C}{B}}\left(\frac{Q}{4}\left(S(x_S)(1-\alpha_S) + \frac{C}{B}(1-\alpha_p(x_S))\right) - (B+C)T_S\right). \tag{2.7}$$

This equation can be solved in the range $x_S \in [0,1]$, which yields the radiative forcing which equilibrates absorbed solar radiation and outgoing longwave radiation for a given latitude of the ice edge $x_s$. Finally, the difference to a reference radiative forcing $A_0$ is considered, $\Delta A = A_0 - A$. This can be seen as the increase of radiative forcing due to an increase in greenhouse gases. The bifurcation diagram resulting from this solution is depicted in Figure 2.2, where solid lines indicate stable solutions and dashed lines unstable solutions.

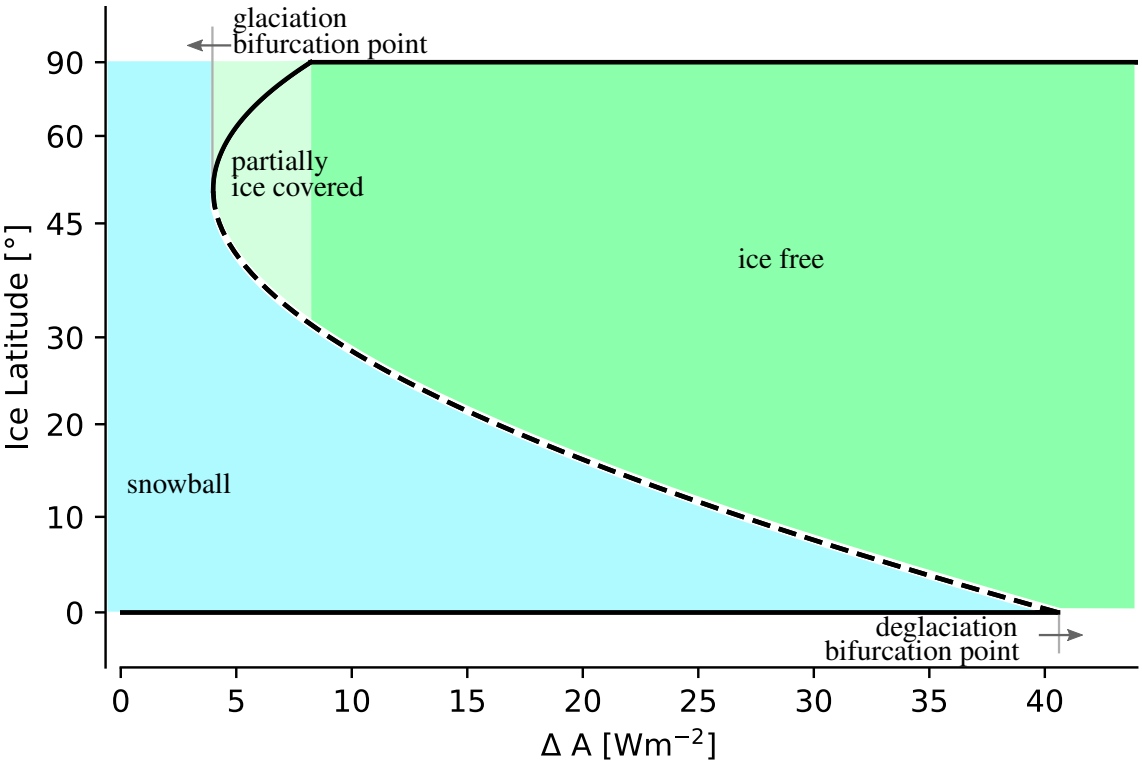


Figure 2.2: Bifurcation diagram of the Budyko-Sellers model. Stable solutions are depicted with a continuous line, unstable solutions with a dashed line. Dark green areas indicate development towards an ice free state, light green towards a partially ice-covered state and blue towards a Snowball state. The locations of the bifurcation points (tipping points) for glaciation and deglaciation are depicted in grey. Constants used as in Abbot et al. (2011): $A_0 = 210\,\mathrm{W\,m^{-2}}$, $B = 1.5\,\mathrm{W\,m^{-2}\,K^{-1}}$, $C = 3.75\,\mathrm{W\,m^{-2}\,K^{-1}}$, $Q = 1285\,\mathrm{W\,m^{-2}}$, $\alpha_1 = 0.3$, $\alpha_2 = 0.6$, $T_S = -10\,^{\circ}\mathrm{C}$.

The life cycle of Snowball Earth described in Section 2.1 can be reproduced by tracing the path a system would take through the diagram by reacting to varying amounts of radiative forcing. Starting with a high value of radiative forcing, there is only an ice free solution with the ice latitude at 90°, because the Earth is too warm for ice to emerge at the poles. This solution is stable against fluctuations of the ice edge, as a lower ice edge would mean that the system now has a higher radiative forcing than the solution for this new ice edge, resulting in the retreat of ice. If radiative forcing is reduced, the system stays in this stable ice free state until it reaches a certain threshold. From here on, ice starts to grow and the system is in a stable partially ice-covered state, similar to today's climate. However, by further decreasing the radiative forcing, a bifurcation point can be reached. By surpassing this point, the system becomes unstable. Earth gains a decreasing amount of energy by the higher planetary albedo and subsequent decrease in absorbed solar radiation. It also loses less energy by less outgoing longwave radiation due to lower temperatures. However, the second effect is smaller. This leads to a runaway ice-albedo feedback: the temperature falls, which leads to ice growth, which increases the global albedo. Less solar radiation is absorbed, which leads to further falling temperature and so on. This continues until a stable equilibrium with global ice cover and extremely low temperatures is reached: the Snowball Earth. For this Snowball Earth to be terminated, the radiative forcing has to increase substantially, up to the deglaciation tipping point where ice starts to melt at the equator. From here on, the same runaway ice-albedo feedback leads to global deglaciation.

The unstable solution separating the regions where the system would develop into a Snowball Earth (blue in Figure 2.2) from the regions where it would develop into an ice free or partially ice-covered state (light/dark green in Figure 2.2) is called the separatrix, depicted as a dashed line in Figure 2.2. This shows the hysteresis in the system: two stable equilibria exist with the same amount of radiative forcing: the Snowball Earth and the ice-free/partially ice-covered state. However, to transition from one state into another, one of the bifurcation points have to be passed. To transition from the ice-free/partially ice-covered climate to a Snowball Earth, radiative forcing has to drop below the glaciation tipping point. To transition from a Snowball Earth to an ice-free climate, radiative forcing has to increase beyond the deglaciation tipping point.

The positions of these tipping points are therefore important for the theory of Snowball Earth. They indicate how much of a decrease in radiative forcing was necessary to initiate the Snowball Earth in the first place. Additionally, they indicate how much radiative forcing had to increase again to terminate the Snowball Earth.

### The Jormungand State

The Jormungand state, which could explain the survival of life during the Snowball climate, can be shown in this model if the ice albedo is further differentiated into two separate values for snow-covered and bare sea ice (Abbot et al., 2011). The ice albedo $\alpha_2$ varies between a higher, snow-covered value $\alpha_2^s$ and a lower, bare ice value $\alpha_2^i$ in a transitional region between $x_i$ and $x_i + \Delta x_i$. This region lies in the subtropics, where a negative surface water balance is assumed, which results in no snow accumulating on the ice surface:

$$\alpha_2(x) = \alpha_2^i + \frac{\alpha_2^s - \alpha_2^i}{2}\left(1 + \tanh\left(\frac{x - x_i}{\Delta x_i}\right)\right). \tag{2.8}$$

This is used to calculate the global mean albedo $\alpha_p(x_s)$ and the albedo at the ice latitude $\alpha_s$ and inserted in equation 2.7. The solution of this adapted equation is depicted in Figure 2.3. It reveals an additional stable state with the ice edge in the tropics, which is separated from the other states by two additional bifurcation points. This so called Jormungand state (Abbot et al., 2011) is stabilized by the albedo contrast between snow-covered and bare ice.

The lower albedo of bare ice in comparison to snow-covered ice weakens the ice-albedo feedback up to the point that the runaway feedback is stopped in the tropics.

For the Jormungand state to be a plausible theory for a Neoproterozoic Snowball Earth, its accessibility is important. This is given with this choice of parameters: the Jormungand state can be reached from a partially ice-covered state by decreasing the radiative forcing and surpassing the glaciation tipping point. If the parameters are changed, however, the Jormungand state can become inaccessible (red in Figure 2.3). This means that if radiative forcing in a partially ice-covered state would be decreased, the Earth would directly fall into a Snowball state, because the hidden Jormungand state only exists at higher $CO_2$ values. Correspondingly, by increasing radiative forcing in a Snowball state until deglaciation start, the Jormungand state will not be reached because it only exists at lower $CO_2$ values. In this case, the likeliness of a Jormungand state existing during the Neoproterozoic is very low, because it would have been extremely difficult to reach this state.

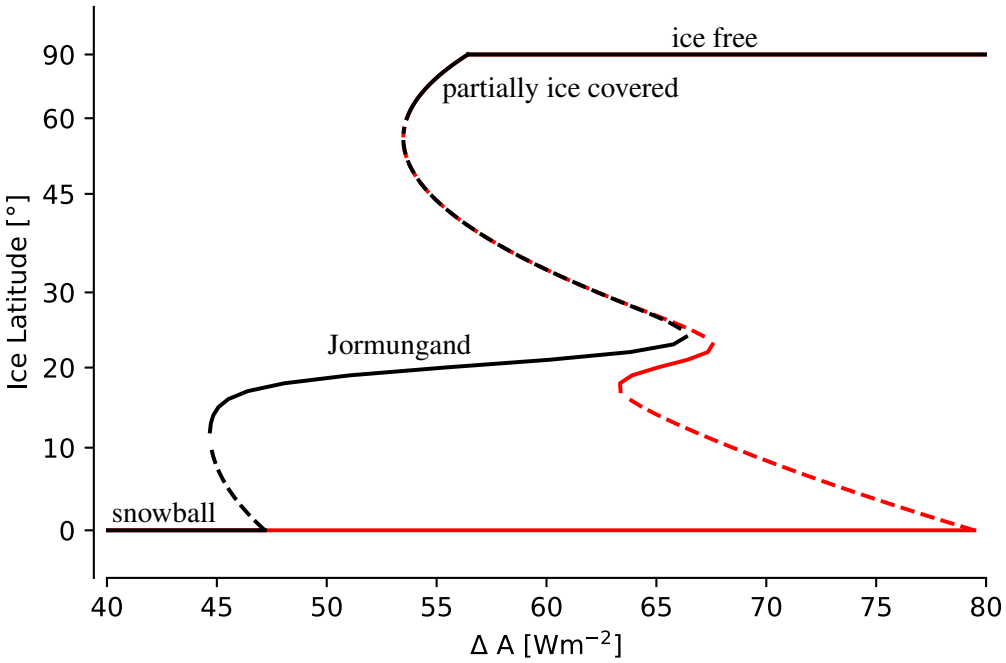


Figure 2.3: Bifurcation diagram of the Budyko-Sellers Model with the Jormungand modification, adapted from Abbot et al. (2011). Stable (unstable) solutions are depicted as solid (dashed) lines. Black lines show the solution with an albedo of ice and snow $\alpha_2^i = 0.45$ and $alpha_2^s = 0.8$. Red lines show the solution for a higher ice albedo of $\alpha_2^i = 0.65$, which results in a inaccessible Jormungand state. All other constants are the same as in Figure 2.2.

## 2.3 Snowball Earth in General Circulation Models

Studies of Snowball Earth have been conducted by simulating the Neoproterozoic climate using ocean and atmospheric models, as well as coupled models. Thereby it can be investigated how Snowball initiation and termination is influenced by different components and processes of the Earth system, and their representation in models. This provides information about how the climate and the Earth in general may have looked like during the Neoproterozoic pan-glaciations. Although the details vary greatly between different studies, the general aspects that are important for this study are briefly summarized in this section.

### Climate of a Snowball Earth

As described by Pierrehumbert et al. (2011), the climate of a Snowball Earth is radically different from today's Earth and more similar to the climate of Mars. This is because the ice cover with a thickness between 800 m and 3000 m eliminates the thermal inertia of the ocean, thus resulting in an extreme seasonal temperature cycle. Because of this, the intertropical convergence zone (ITCZ) is subject to large seasonal fluctuations in the north-south direction, resulting in an effectively reversed hydrological cycle with net ablation in the tropics and atmospheric water transport from the tropics into the subtropics. Generally cold temperatures (as low as $-130\,^{\circ}\mathrm{C}$ at the surface of the poles) result in the atmosphere showing an extremely low water content, effectively eliminating the impact of water vapor as a greenhouse gas. Clouds, however, are present and play an important role in warming the Earth by the longwave cloud-radiative effect of high-level clouds (Abbot et al., 2012).

### Sea-Ice Dynamics

A Snowball Earth would be covered by extremely thick sea ice. Furthermore, sea ice is responsible for changing the surface albedo and thus is the reason why the Snowball Earth Bifurcation exists in the first place. An appropriate representation of the vast sea-ice cover is therefore of importance.
One aspect is the dynamics of sea ice. Voigt and Abbot (2012) showed that sea-ice dynamics increase the $CO_2$ amount required for Snowball initiation by a factor of 100, therefore strongly enhancing Snowball initiation. This is due to the fact that the thick sea ice in the higher latitudes results in a high ice pressure that results in ice flowing towards the equator. This is further enhanced by trade winds in the subtropics, which exert a surface stress on the sea ice, resulting in an equatorward motion. A counteracting but weaker factor is ocean dynamics, where ocean currents from the equator towards the poles result in a drag on the sea ice away from the equator.
In total, sea ice is transported towards the equator, which strongly enhances Snowball initiation due to ice being present at lower latitudes. This does not only push the bifurcation point to a much higher $CO_2$ level, but also prevents a stable Jormungand state.

### Sea-Ice Albedo

Due to the ice-albedo feedback playing a central role for Snowball Earth, the albedo of ice and snow surfaces have an enormous impact on simulations of Snowball Earth. The higher the albedo

difference between ice and ocean, the stronger the ice-albedo feedback and the larger the associated Snowball bifurcation (cf. Sec. 2.2), and vice versa.

Increasing the snow albedo from 0.65 to 0.75 enhances the ice-albedo feedback in such a way, that atmospheric $CO_2$ content has to be up to 8 times higher for deglaciation to occur (Lewis et al., 2006). The same effect happens for glaciation, where an increase of ice albedo from 0.60 to 0.65 leads to doubling of the atmospheric $CO_2$ content, which still allows for glaciation to occur (Yang et al., 2012).

Albedo is thus a central factor in simulations of Snowball Earth. The albedo values defined in the parameterization of the ice cover can therefore influence the position of the Snowball Bifurcation. Additionally, surface melting of ice and snow decreases albedo by replacing brighter dry ice or snow with darker wet ice or snow.

### The Melt-Ratchet Effect

The melt-ratchet effect decreases the surface thickness of ice in simulations of Snowball Earth both on a diurnal and a yearly scale (Pierrehumbert et al., 2011). Its course is depicted in Figure 2.4: sea ice exists on top of the ocean. During summer or during the day, melting takes place on the surface due to warm temperatures and high incoming solar radiation. This reduces the ice thickness. The melt water forms melting ponds on top of the ice. However, these ponds can be removed by drainage or evaporation. In fact, surface melting doesn't even lead to melting ponds in simple ice models, as melt water is not considered (Semtner (1976), Winton (2000)). If the melt water is thus removed, there is nothing to refreeze at the surface during winter or night. Instead, only freezing from the bottom can take place. However, the bottom growth is significantly weaker than the preceding melting at the top, because the diffusion of heat is dampened by the thickness of ice. Consequently, the melt-ratchet effect leads to a net decrease of ice thickness on a daily and a seasonal scale. A larger daily or seasonal cycle of surface temperatures increases the total ablation, because more ice will melt during the day or during the summer (Abbot et al., 2010).

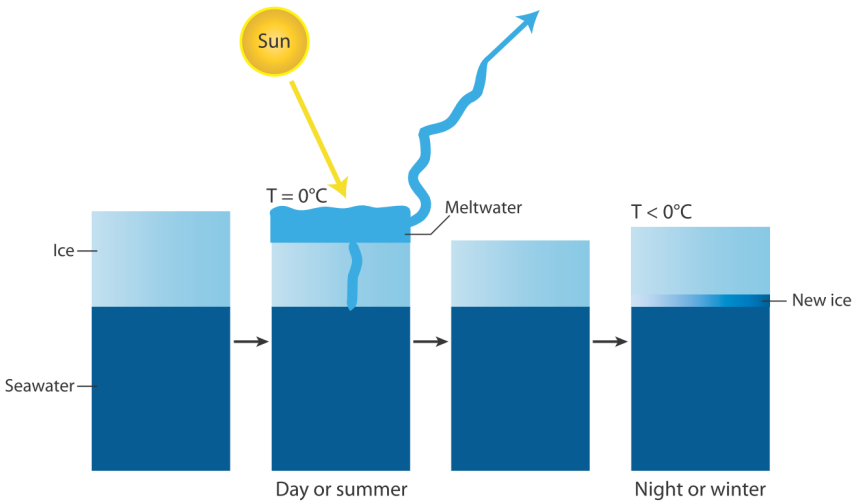


Figure 2.4: Schematic representation of the melt-ratchet effect. Figure taken from Pierrehumbert et al. (2011).

### Sea-Ice Vertical Resolution

The vertical resolution of sea ice has a major impact on the melt-ratchet effect and Snowball termination. Abbot et al. (2010) tested the impact of vertical ice resolution on Snowball termination, using a Semtner model with 2, 4 and 60 levels. Increasing the vertical resolution of sea ice increases the effective heat capacity. Consequently, the daily cycle of surface temperatures is dampened: the surface temperature is higher at night and lower at noon. This weakens the melt-ratchet effect, because less ice is melting during the day. It is therefore much more difficult for ice to melt having a higher resolution. This can be seen in Figure 2.5. With 60 vertical levels, no melting takes place at all. Decreasing the amount of levels to 4 or 2 increases the melt occurring each day, resulting in a gradual decrease of sea-ice thickness each day.

For Snowball termination, this means that an increased vertical resolution of sea ice impedes deglaciation. Significantly more $CO_2$ is thus required for ice to start melting at the equator due to the logarithmic dependence of radiative forcing on $CO_2$. The deglaciation tipping point of the Snowball bifurcation is thus pushed towards higher $CO_2$ values.

Yang et al. (2012) discovered the same effect for Snowball initiation: Increasing the number of vertical ice layers results in faster glaciation, due to colder surface temperatures and less surface melting.

Curry et al. (1995) tested the local ice-albedo feedback for polar ice sheets. Here, a Semtner 3-layer model and a Semtner 0-layer model are compared. The 0-layer Semtner model completely neglects heat capacity (Semtner, 1984), which further increases the daily temperature cycle and thus surface melting. This results in a more intense ice-albedo feedback using the 3-layer model in comparison to using the 0-layer model. This is due to the 3-layer model causing a larger sea-ice cover, as well as effects in multiyear pack ice such as a longer lasting snow cover on the ice due to less efficient surface melting. This phase difference of ice and snow thickness between 0-layer

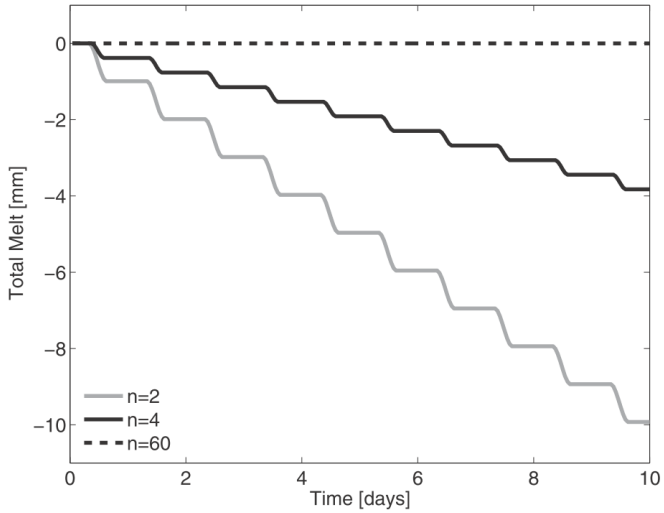


Figure 2.5: Time series of total surface melt using a Semtner sea-ice model with 2, 4 and 60 vertical levels forced by identical idealized boundary conditions. The qualitative behaviour of the melt-ratched effect is independent of the choice of these boundary conditions. The melt-ratched effect can be seen in the gradually decreasing sea-ice thickness at noon. Figure taken from Abbot et al. (2010)

and 3-layer models results in a snow cover that is present longer into the summer using a 3-layer model, reflecting more solar radiation as a consequence.
Generally speaking, a higher vertical resolution of ice enhances the ice-albedo feedback due to less efficient surface melting. This effect has been shown in investigations of current polar ice sheets as well as in Snowball climates. For a Snowball Earth, however, this effect is expected to have a much higher impact due to the global presence of ice. Consequently, increased vertical resolution should result in enhanced glaciation and impeded deglaciation of Snowball Earth.

# 3 Research Questions

In this chapter, the research questions that are answered in this thesis are formulated. The results of the first research question are presented in Chapter 5, the results of the second question in Chapter 6.

## 3.1 Impact of Sea-Ice Thickness Limitation

Sea-ice schemes in coupled ocean-atmosphere models often set a maximum thickness of sea ice to avoid problems in the ocean model when the sea-ice becomes too thick and the uppermost ocean level risks to become fully filled with sea-ice. This has also been done in studies of Snowball Earth that used a coupled ocean-atmosphere model (e.g Voigt et al. (2011), Voigt and Abbot (2012)). In the ICON-AES model, such a sea-ice thickness limitation is not necessary, because it uses a mixed-layer ocean without ocean dynamics.

For modern-day climate, where only a thin sea-ice cover exists, a thickness limit is not a severe restriction. In Snowball Earth climates however, sea ice can reach an enormous thickness of several hundred meters, due to extremely low surface temperatures (Pierrehumbert et al., 2011). In this case, an artificially thin sea-ice cover of only 5 m is a major restriction. The warm ocean - that can only be as cold as its freezing temperature - is now separated from the extremely cold atmosphere by an ice cover only 5 m thick. As a consequence, the heat flux from the ocean into the atmosphere will be artificially increased. This flux constantly heats the atmosphere, growing larger the more ice exists and the colder the atmosphere is.

At the Snowball Earth Bifurcation, the climate system shows strong nonlinear behaviour, especially in vicinity of the glaciation tipping point. An addition of an artificial heat flux into such an unstable system can thus potentially have a large impact. In the first part of this thesis, the magnitude of this effect will be determined, answering the question:

> How does a sea-ice thickness limitation of 5 m impact the initiation of Snowball Earth in ICON?

## 3.2 Impact of Increased Vertical Resolution

The vertical resolution of sea-ice schemes has a substantial impact on local ice physics. Simple models with 0 vertical layers neglect the heat capacity of ice (Semtner, 1984). This modifies the amplitude and the phase of the surface temperature cycle (Curry et al., 1995). Consequently, melting at the ice surface is affected.

Increasing the amount of vertical layers to 3 adds a heat capacity. This dampens the temperature cycle and therefore decreases surface melting (Semtner, 1984). The melt-ratchet effect, which is responsible for gradually decreasing ice thickness, is thus weakened. On a multiyear scale, this enhances ice growth.
Additionally, the decreased surface melting and the introduced phase lag leads to increased reflected radiation, because snow with higher albedo will melt more slowly, resulting in a snow cover persisting longer into the summer (Curry et al., 1995).
In Snowball climates, where the ice-albedo feedback plays a pivotal role, this change in ice surface effects can have a strong impact. An increase in the vertical resolution both impedes deglaciation (Abbot et al., 2010) and enhances glaciation (Yang et al., 2012). In the second part of this thesis, the influence on the initiation of a Snowball Earth will be further investigated, answering the question:

How does the vertical resolution of the sea-ice scheme impact the initiation of Snowball Earth in ICON?

# 4 Methods

This chapter sets out the methods used in this thesis to answer the research question. Section 4.1 describes the sea-ice schemes that are applied in the investigations. Section 4.2 then provides information about the ICON-AES model that is used and its model set-up. Lastly, Section 4.3 describes the implementation of the sea-ice schemes in offline Python simulations.

## 4.1 Sea-Ice Schemes

Modern sea-ice schemes applied in general circulation models can have various degrees of complexity, including dynamical, thermodynamical and biochemical processes (Notz and Bitz, 2016). In this thesis however, only thermodynamic models are considered: A Semtner model in a 0-layer version and a 3-layer reformulated Winton model. In these models, the driving factors are the energy balances at the atmosphere-ice and ice-ocean surface, which determine the heating rate and the resulting change in ice thickness and temperature. Additional factors that are considered are ice salinity and penetrating radiation in the case of the reformulated Winton model, which leads to internal melting and emergence of brine pockets.
Both models are first described in the way they are used in this thesis, followed by a conceptual comparison between both models.

### 4.1.1 Semtner Model

The sea-ice model by Semtner (1976) is a simplification of the thermodynamic sea-ice model by Maykut and Untersteiner (1969, 1971). It considers the vertical heat fluxes through the ice using any number of layers. Here we apply a so-called 0-layer version of the Semtner model, in which no internal temperatures are predicted and the ice thus has zero heat capacity. Additionally, penetrating radiation and brine pockets are not considered.
The 0-Layer Semtner Model (Fig. 4.1), from here on called Semtner Model unless stated otherwise, considers the conductive heat flux $F_S$ through sea-ice and snow depending on the temperature gradient between ocean and atmosphere:

$$F_S = \frac{k_S(T_B - T_S)}{h_S + \left(\frac{h_I k_S}{k_I}\right)}, \tag{4.1}$$

with $T_B = -1.9\,^{\circ}\mathrm{C}$ being the constant ocean temperature and $T_S$ the surface temperature. $h_S$ and $h_I$ are the snow and ice thickness. $k_S$ and $k_I$ are empirical values for the thermal conductivities of snow and ice.
The surface temperature $T_S$ is calculated by using a flux balance between the ice heat flux and atmospheric heat flux:

$$F_S + F_A = 0. \tag{4.2}$$

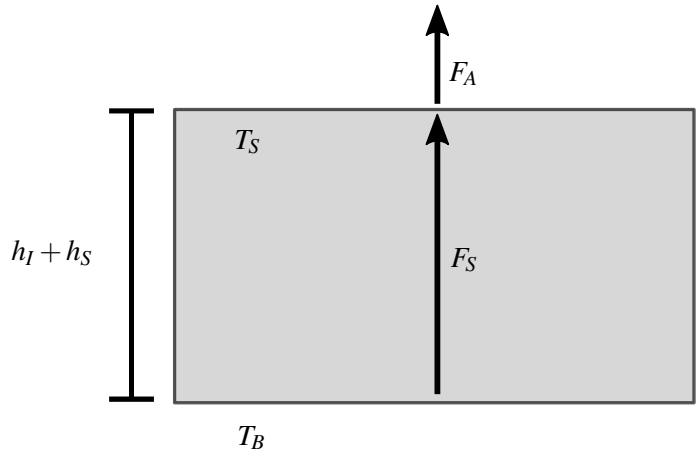


Figure 4.1: Schematic structure of the Semtner Model.

The atmospheric heat flux $F_A$ is composed by the latent heat flux $F_l$, the sensible heat flux $F_t$, the incoming longwave $F_L$ and shortwave radiation $F_r$ as well as the outgoing longwave radiation described by the Stefan Boltzmann equation $\sigma T_S^4$:

$$F_A = F_l + F_t + F_L + (1 - \alpha_S)F_r + \sigma T_S^4. \tag{4.3}$$

Incoming shortwave radiation is decreased by the surface albedo $(1 - \alpha_S)$.

### Thickness change

If the surface temperature resulting from the surface energy balance is above the melting point, the ice at the surface melts while the surface temperature is held constant at $T_S = 0\,^{\circ}\mathrm{C}$.

For snow-covered ice, the thickness of the snow cover changes by:

$$\frac{\Delta h_S}{\Delta t} = \frac{F_A - F_S}{L\rho_S} \tag{4.4}$$

and for bare sea ice, the ice thickness is changed instead:

$$\frac{\Delta h_I}{\Delta t} = \frac{F_A - F_S}{L\rho_I}. \tag{4.5}$$

$L$ is the specific enthalpy of fusion for water in $\mathrm{J\,kg^{-1}}$, $\rho_I$ and $\rho_S$ are the densities of ice and snow. The heat flux available for surface melting can thus be defined as:

$$qtop = F_S - F_A. \tag{4.6}$$

At the bottom of the ice layer, ablation or accretion is governed by the heat flux through the ice $F_S$, which transfers energy from the ocean in the atmosphere:

$$\frac{\Delta h_I}{\Delta t} = \frac{F_S}{L\rho_I}. \tag{4.7}$$

The heat flux available for bottom melting can thus be defined as:

$$qbot = -F_S. \tag{4.8}$$

### Snow-to-Ice Conversion

As the Semtner Model predicts unrealistically high values of snow thickness (Mitra and Das, 2007), a snow-to-ice conversion can be included. If the snow cover is heavy enough to push the sea ice completely under water, the amount of snow below the water surface is converted to ice. The depth of snow below water is calculated by:

$$h_{below} = \frac{\rho_I h_I + \rho_S h_S}{\rho_W} - h_I, \tag{4.9}$$

with the densities of ocean water $\rho_W$. This results in the following for the new ice thickness:

$$h_{I,new} = h_I + h_{below} \tag{4.10}$$

and for the new snow thickness:

$$h_{S,new} = h_S - \frac{\rho_s}{\rho_i} h_{below}. \tag{4.11}$$

The density corrections in Equations 4.9 and 4.11 allow a mass-preserving transformation of snow into ice.

### Limitation of Sea-Ice Thickness

Using the Semtner 0-layer model, sea-ice thickness can be limited to a maximum value. Such a limitation is common in simulations that use a coupled ocean model, because problems can arise in the ocean model if the sea ice grows thick enough so that the whole upper ocean layer consists of ice.

To avoid sea ice from growing too thick, the sea-ice thickness is limited to its maximum value at the end of the sea-ice scheme:

$$h_I = \min\left(h_I, h_{I,max}\right). \tag{4.12}$$

In combination with the conversion of snow to ice, this also limits the snow thickness.

Without this limitation, the sea ice would grow indefinitely, as long as the average surface temperature is below the freezing point. To verify this, Equation 4.1 can be inserted into Equation 4.7, which results in the instantaneous change in ice thickness:

$$\frac{\mathrm{d}h_I}{\mathrm{d}t} = \frac{1}{L\rho_I}\left(\frac{k_S(T_B - T_S)}{h_S + \left(\frac{h_I k_S}{k_I}\right)}\right). \tag{4.13}$$

Assuming constant surface temperature $T_S$ and ocean temperature $T_B$, as well as a snow height of 0 m, equation 4.13 can be integrated:

$$\int h_I \, \mathrm{d}h_I = \int \frac{k_I(T_B - T_S)}{L\rho_i}) \, \mathrm{d}t \tag{4.14}$$

$$h_I(t) = \sqrt{\frac{2k_I(T_B - T_S)}{L\rho_i}t} \tag{4.15}$$

$$h_I(t) \propto \sqrt{t}. \tag{4.16}$$

Correspondingly, no equilibrium ice-thickness exists in this setup of the Semtner model.
To prevent the ice thickness from growing infinitely and interfering with the ocean model, the maximum sea-ice thickness is set to $h_{i,max} = 5\,\mathrm{m}$ in the Semtner-limited simulations performed in this thesis.
However, using a mixed-layer ocean, such a limitation is not necessary, the slab ocean can never run dry by design. In fact, in the climate of a Snowball Earth, such a limitation can affect the atmospheric energy balance by causing an artificially high heat flux from the ocean into the atmosphere, due to surface temperatures that reach extremely low values with only a thin ice layer dampening the heat flux.

### 4.1.2 Winton Reformulated 3-Layer

Winton (2000) reformulated the 3-level Semtner model with a physically more accurate representation of brine content and a more efficient time stepping scheme. In this section, the most important characteristics of the Winton ice scheme as implemented in the ICON model are described, with adapted notations for better comparability with the Semtner 0-layer model. For a more detailed description see Winton (2000).
The basic assumption is that sea ice conserves an enthalphy:

$$E(T) = C(T + \mu S) - L\left(1 + \frac{\mu S}{T}\right), \tag{4.17}$$

with the heat capacity $C$, the temperature $T$ (in °C), the constant ice salinity $S$, the latent heat of fusion $L$ and a constant for the linear relationship between salinity and the melting point $\mu$. $E(T)$ is equivalent to the energy per mass that is stored in ice with a certain temperature, $E(T)$ is thus negative for ice temperatures below the freezing point and $-E(T)$ corresponds to the energy that is required to melt the ice. The ice salinity $S = 5\,\mathrm{ppt}$ and the relation to freezing temperature $\mu = 0.054\,^{\circ}\mathrm{C\,ppt^{-1}}$ result in $\mu S = 0.27\,^{\circ}\mathrm{C}$, which corresponds to the reduction of the ice melting temperature by the ice salinity. $-\mu S$ is therefore the melting temperature of ice with the salinity $S$.
This approach allows for an implicit representation of brine pockets in the ice and their effect on ice heat capacity. The factor $\frac{\mu S}{T}$ in Equation 4.17 represents the amount of enthalpy that is stored in liquid brine pockets instead of the ice. The brine content of the ice is thus completely determined by the ice temperature. Ultimately, this means that heating the ice results in a smaller temperature change than without brine pockets, so brine pockets increase the effective heat capacity of the ice (see Bitz and Lipscomb (1999) for the derivation and further explanations).

Following this, the heating of ice results in two effects: changing of temperature or changing of brine content. The heat capacity of the ice is therefore not constant and changes via a change in brine content. Heating of ice with the mass $m$ with the flux $F$ thus results in the following enthalpy change:

$$m\frac{dE}{dt} = m\left(C + \frac{L\mu S}{T^2}\right)\frac{dT}{dt} = F \tag{4.18}$$

The Winton Model divides the ice into 3 layers, two ice layers and one snow layer (Figure 4.2). The two ice layers have the same thickness, because they are evened at the end of each time step. The snow layer is assumed to have no heat capacity, because it is negligibly small. The upper ice layer has a variable heat capacity, due to brine pockets that form by penetrating radiation ($I$ in Figure 4.2), so the enthalpy balance in equation 4.17 is used. The lower ice layer is assumed not to be reached by penetrating radiation. Due to this, no brine pockets can form, so the factor $\frac{\mu S}{T}$ in Equation 4.17 can be neglected. The enthalpy of this layer can therefore be simplified:

$$E_2(T) = C(T + \mu S) - L \tag{4.19}$$

and the enthalpy change is written as:

$$m\frac{dE_2}{dt} = mC\frac{dT}{dt} = F. \tag{4.20}$$

Apart from the different calculations for enthalpy and penetrating solar radiation, the two ice layers have identical properties. Using the enthalpy of each ice layer and the heat fluxes between them as well as into the atmosphere and into the ocean, the internal ice temperatures and the resulting thickness change can be calculated.

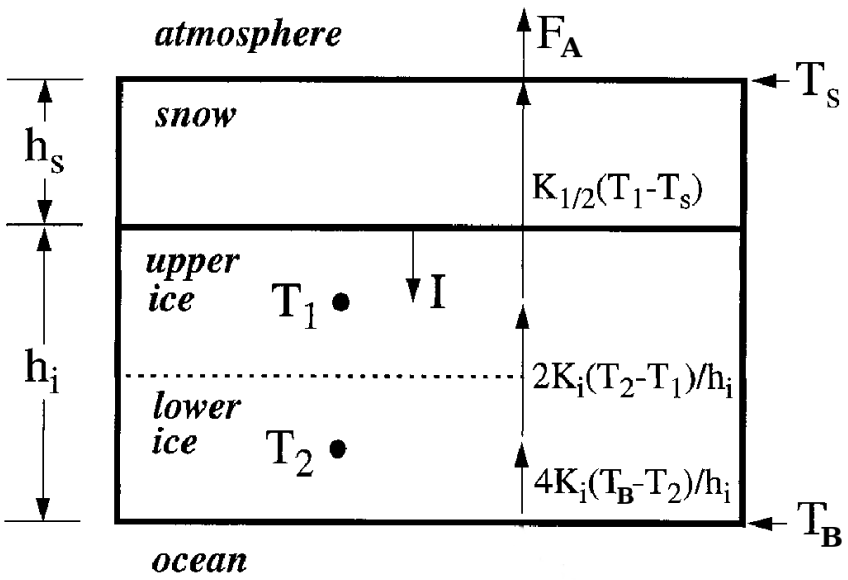


Figure 4.2: Schematic structure of the Winton Model, adapted from Winton (2000). The surface temperature $T_S$ is calculated via the surface energy balance. The bottom temperature $T_B$ is fixed at the freezing point of ocean water. The internal heat fluxes are determined by the temperatures and the conductivity of ice $K_i$ and the snow-ice coupled conductivity $K_{1/2}$ (Equation 4.22).

There are therefore 4 prognostic variables: the snow thickness $h_S$, the ice thickness $h_I$ and the ice layer temperatures $T_1$ and $T_2$ (cf. Figure 4.2). The thickness of each layer is not predicted, as each thickness is always set to $\frac{h_I}{2}$ at the end of each time step.

### Temperature calculation

The heat flux $F_A$ from the surface into the atmosphere is calculated in the same as in Semtner, using a surface energy balance (Equation 4.3). The surface temperature $T_S$ is then calculated using the flux balance of the flux into the atmosphere and the flux into the ice or snow, defined as:

$$F_S = K_{1/2}(T_1 - T_S), \tag{4.21}$$

with the thermal conductivity $K_{1/2}$ that couples the conductivities of the snow layer $K_S$ and the upper ice layer $K_I$:

$$K_{1/2} = \frac{4K_I K_S}{K_S h_I + 4K_I h_S}. \tag{4.22}$$

The heat flux between the ice layers is defined accordingly as:

$$F_1 = K_I \frac{T_2 - T_1}{\frac{1}{2}h_I}, \tag{4.23}$$

as well as the heat flux at the bottom:

$$F_2 = K_I \frac{T_B - T_2}{\frac{1}{4}h_I}. \tag{4.24}$$

The ice temperatures $T_1$ and $T_2$ are calculated from the balance of these fluxes and penetrating radiation $I$ (see Winton (2000)).

### Thickness change

After the calculation of ice temperatures, the heat flux $F_2$ is recalculated using the updated temperatures. A heat flux available for bottom melting can be defined as:

$$qbot = -F_2. \tag{4.25}$$

This heat flux changes the enthalpy of the lower ice layer calculated by Equation 4.19, which results in melting or freezing of an amount of ice that corresponds to this enthalpy. Ablation or accretion at the bottom of the ice is therefore calculated via:

$$\frac{\Delta h_2}{\Delta t} = \frac{-qbot}{\rho_I E_2(T_B)} = \frac{-qbot}{\rho_i(C(T_B + \mu S) - L)}. \tag{4.26}$$

On the surface, if the temperature calculation results in a surface temperature above the melting point, the surface temperature is set to the freezing point and an excess heat flux $qtop$ is applied, calculated from the updated temperatures:

$$qtop = F_S - F_A. \tag{4.27}$$

This heat flux heat flux thus melts ice or snow, until the surface temperature reaches the melting point. If snow is present on the ice, the snow layer changes by:

$$\frac{\Delta h_S}{\Delta t} = \frac{qtop}{\rho_S L}. \tag{4.28}$$

If no snow is present, the upper ice-layer thickness changes by:

$$\frac{\Delta h_1}{\Delta t} = \frac{-qtop}{\rho_I E(T_1)} = \frac{-qtop}{\rho_I \left(C(T_1+\mu S) - L\left(1+\frac{\mu S}{T_1}\right)\right)}. \tag{4.29}$$

If any layer is molten completely by the heat flux from the top or bottom, the excess heat flux is applied to the melting of the next layer.
Comparing the formulas for thickness change with the Semtner model, it's noticeable that the heat fluxes for bottom ($qbot$) and top ($qtop$) melting are defined similarly in both models. However, the Winton model uses the upper ice temperature $T_1$ for the calculation of the top melting heat flux, while Semtner 0-level uses the ocean temperature $T_B$. Correspondingly for bottom melting, the Winton model uses the lower ice temperature $T_2$, while Semtner uses the surface temperature $T_S$. This demonstrates the fundamental difference between these models: The Semtner 0-layer model is extremely dependent on the surface temperature, which drives both top and bottom processes. The added layers in the reformulated 3-layer Winton model on the other hand add a dampening component, which regulates both top and bottom processes.

### Snow-to-Ice conversion

If the thickness of the snow layer $h_S$ is thick enough to push the ice below water, all snow below the water is converted into upper layer ice in the same way as in the Semtner model (cf. Equation 4.10). If this happens, the upper ice temperature is adjusted to incorporate the snow without heat capacity. This is done by an enthalpy conversion: The enthalpy of the snow that is converted to ice is calculated using Equation 4.19 and added to the enthalpy of the upper ice layer. Using this new enthalpy, the new temperature of the upper ice layer can be calculated using Equation 4.17.

### Equalizing the Ice-Layer Thicknesses

At the end of each time step, ice is transferred between the layers in a way that both layers have the same thickness. Therefore, upper ice with variable heat capacity has to be converted into lower ice with constant heat capacity or vice versa (i.e., brine pockets freeze or ice melts into brine pockets). For this, an enthalpy conversion according to the same principle as for the snow-to-ice conversion is applied.
The enthalpy of the ice that is transferred to the other layer is added to the enthalpy of that layer, and a new ice temperature is calculated (using either Equation 4.17 if ice is transferred from the lower to the upper layer or Equation 4.19 if the other way around).
Finally, it is possible that the lower ice temperature surpasses the melting point due to this ice conversion. To account for this, lower ice is molten until the temperature reaches the melting point again.

### 4.1.3 Conceptual Comparison between the Reformulated 3-Layer Winton Model and the Semtner 3-Layer Model

As the Winton model is a reformulation of the Semtner model in its 3-layer version, the structure of both models is very similar. The main conceptual differences between the Semtner 3-layer model and the Winton 3-layer model are the enthalpy conserving approach of the Winton model, which allows for an implicit calculation of brine content, and the neglect of snow heat capacity. In fact, Winton (2000) showed that both models predict similar seasonal cycles of ice temperatures and ice thickness. Mitra and Das (2007) on the other hand found that the Semtner 3-layer model underestimated the thickness of Antarctic sea ice, while the Winton 3-layer model predicted it more accurately. However, this may be due to the fact that no snow-to-ice conversion was implemented in this Semtner model.
The differences between theses models are all related to changes of the (effective) heat capacity of the ice and snow layer. This heat capacity is completely neglected in the 0-layer Semtner model. For a comparison with the 0-layer Semtner model in terms of vertical resolution, as it is done in this thesis, the difference between Winton 3-layer and Semtner 3-layer can therefore be disregarded.

## 4.2 ICON-AES Model

In this thesis, the general circulation model ICON-AES in version 1.3.00 is used. This is the atmospheric component of the icosahedral nonhydrostatic ICON model (Giorgetta et al., 2018).
The horizontal grid of ICON in general is derived from a spherical icosahedral grid by dividing the original triangles into a number of continuously smaller triangles. The vertical resolution is defined by a terrain following grid.
ICON-AES uses the same dynamical core as other ICON configurations but differs in its physics parameterization. ICON-AES uses physics packages adapted from the ECHAM6 model (Stevens et al., 2013), coupled to the nonhydrostatic dynamical core in a way similar to ECHAM6. As such, ICON-AES is designed for the use in climate simulations, with the option of a very high resolution and a large scalability. It is tuned to the established ECHAM6-LR model in a way to show a well balanced top-of-the-atmosphere energy balance.

### 4.2.1 Simulation Set-Up

For use in climates of Snowball Earth, several adjustments are made. The solar constant is set to $1285\,\mathrm{W\,m^{-2}}$ and Earth has a circular orbit with an obliquity of 23.5°. The length of a year is changed to 360 days. The top two model levels are removed to avoid instability in the extremely cold climate. To further avoid instabilities, the temporal resolution is decreased during the course of each simulation from initially 600 s to 480 s and 360 s. The effective horizontal resolution is 160 km.
All greenhouse gases in the atmosphere are removed except $CO_2$ and water vapor. $CO_2$ is used to control the external forcing, so it is kept constant over the course of one simulation, no processes that change the atmospheric $CO_2$ content are implemented.
The simulations are run with an aquaplanet setup, without any continents. The ocean is a mixed-layer ocean with a depth of 50 m. The mixed-layer ocean does not have any dynamics or lateral

heat fluxes. At every grid point the ocean can change its temperature via surface fluxes. If the surface temperature falls below the freezing point, sea ice forms and the ocean temperature remains constant.

Three sets of simulations are carried out with the same set-up, using different sea-ice models (Section 4.1).

1. **Semtner-limited**: using a Semtner 0-layer sea-ice scheme with a maximum sea-ice thickness of 5 m.

2. **Semtner-unlimited**: using a Semtner 0-layer sea-ice scheme without a sea-ice limit.

3. **Winton**: using a Winton Reformulated 3-layer sea-ice scheme. The sea-ice thickness is unlimited as in the Semtner-unlimited simulations.

Each simulation is initialized with a certain constant atmospheric $CO_2$ content and specific initial conditions in terms of atmospheric variables and sea-ice cover. Simulations that are started from an ice-free state use initial conditions derived from the AMIP simulations from Giorgetta et al. (2018), modified to an aqua planet without any ice and a mixed layer ocean with zonally symmetric sea surface temperatures. Simulations that are started from any other state use restart files of previous simulations as initial conditions. These allow for simulations to start from a Jormungand-like state, where there already exists an ice cover up to a lower latitude, or a partially ice-covered state, to save computing time.

The Semtner-limited simulations were performed beforehand by Christoph Braun, in connection to other work, whereas the Semtner-unlimited and Winton simulations are performed during this thesis as a comparison.

A central part of this thesis is the construction of the Snowball Earth bifurcation diagram for the simulations using the three different sea-ice schemes. By investigating the bifurcation and the differences occurring using the different sea-ice schemes, the physical impact of the sea-ice schemes can be determined. The starting and ending points of the simulations are therefore entered into an ice latitude - atmospheric $CO_2$ diagram, from which the bifurcation diagram can be constructed.

The ice latitude is calculated from the global sea-ice cover *sic*. The ice is assumed to be symmetric with respect to the equator, forming a continuous ice cover from the poles down to one specific latitude. Thus the latitude of the sea-ice edge can be calculated by:

$$\text{ice latitude} = \arcsin\left(1 - sic\right). \tag{4.30}$$

The main characteristics based on which the simulations are compared are the direction in which the sea-ice edge develops, i.e., if the system changes towards an ice free or a Snowball Earth, as well as the velocity of the sea-ice edge change. Additional important variables are the heat fluxes available for top and bottom melting $qtop$ and $qbot$, as well as surface temperature and surface albedo.

## 4.3 Offline Sea-Ice Models with Idealized Boundary Conditions

To enable a more detailed study of the physical differences between the sea-ice schemes, the Semtner-unlimited and Winton models are rewritten using python. In this way they can be run outside of the ICON model using idealized boundary conditions.
These models consist of one grid point, at which all physical processes described in Section 4.1.1 and 4.1.2 responsible for governing the growth and ablation of sea-ice are simulated. The models take ice thickness, snow thickness, ice surface temperature (and internal ice temperatures in case of Winton) as initial conditions and use the atmospheric fluxes (shortwave & longwave radiation, sensible & latent heat) into the ice surface as forcing during the model run. The time step of the forward integration is set to 600 s, corresponding to the initial time step of the ICON model runs. All physical constants are taken from the sea-ice models in ICON, to guarantee the comparability of the ice physics.
Running the Semtner-unlimited and Winton models with the same initial conditions and forcing allows for a clear visualization of the different ice physics.

# 5 Impact of Sea-Ice Thickness Limitation

This chapter presents the results of the first research question: How does a sea-ice thickness limitation of 5 m impact the initiation of Snowball Earth in ICON? Firstly, the simulations that were performed using a 0-layer Semtner model with unlimited sea-ice thickness are described in Section 5.1. The evolution of the sea-ice edge is investigated to determine the position of the Snowball Earth bifurcation point and the location of the separatrix. In Section 5.2, these results are compared with the simulations using a Semtner 0-layer model with limited sea-ice thickness. The artificial heat flux resulting from the limitation is derived and investigated. Finally, Section 5.3 summarizes and discusses the results by displaying the effects of the sea-ice thickness limitation on the bifurcation diagram.

## 5.1 Evolution of the Sea-Ice Edge

The Semtner-unlimited simulations carried out and investigated are listed in Table 5.1 They can be divided into two groups: simulations started from an ice-free or temperate partially ice-covered state and simulations started from a Jormungand-like state.
In Section 5.1.1, the simulations started from an ice-free or partially ice-covered state are investigated. The simulations started from a partially ice-covered state (SU_1594 and SU_1688) use a restart file after 100 years of another simulation with a higher $CO_2$ content (SU_1875) for initial conditions. This was done to save computing time. It is safe to assume that this only has a marginal effect on the course of the simulation and especially its the final stable position of the ice edge. This is due to the fact that these simulations have a lower $CO_2$ content than the one which produced the restart file, which means that they will result in a stable ice edge at a lower latitude. Consequently, at some point they have to be in a state with the same ice latitude than the restart file of the simulation with higher $CO_2$ content.
Afterwards in Section 5.1.2, the simulations started from a Jormungand-like state are investigated. Lastly, selected Semtner-unlimited and Semtner-limited simulations are compared to quantify the effects of the sea-ice thickness limitation.

Table 5.1: List of all Semtner-unlimited simulations performed. The $CO_2$ content is constant throughout the simulation. Start and end ice latitude refers to the latitude of the sea-ice edge at the start and end of the simulation, 90° being ice free and 0° a Snowball Earth. Start and end year refers to the internal mode time. When the start year is larger than 1, the simulation was started from a restart file from that year of another simulation, listed in the initial conditions. Otherwise it was started from ice-free initial conditions (cf. Section 4.2.1).

| simulation name | $CO_2$ content | start ice latitude | end ice latitude | start year | start year | initial conditions |
|---|---|---|---|---|---|---|
| SU_1500 | 1500 ppmv | 90° | 0° | 1 | 320 | aqua-icefree |
| SU_1594 | 1594 ppmv | 53.02° | 49.54° | 100 | 230 | SU_1875 |
| SU_1688 | 1688 ppmv | 53.02° | 51.07° | 100 | 190 | SU_1875 |
| SU_1875 | 1875 ppmv | 90° | 53.20° | 1 | 150 | aqua-icefree |
| SU_2250 | 2250 ppmv | 90° | 56.85° | 1 | 150 | aqua-icefree |
| SU_3000-22lat | 3000 ppmv | 22.05° | 22.83° | 400 | 600 | SU_5000-14lat |
| SU_3000-14lat | 3000 ppmv | 14.46° | 0° | 291 | 340 | SU_1500 |
| SU_3750-19lat | 3750 ppmv | 19.29° | 18.73° | 400 | 600 | SU_5000-14lat |
| SU_3750-14lat | 3750 ppmv | 14.46° | 0° | 291 | 448 | SU_1500 |
| SU_3907-14lat | 3907 ppmv | 14.46° | 15.09° | 291 | 350 | SU_1500 |
| SU_4063-14lat | 4063 ppmv | 14.46° | 11.57° | 291 | 509 | SU_1500 |
| SU_4219-14lat | 4219 ppmv | 14.46° | 16.28° | 291 | 58 | SU_1500 |
| SU_4375-14lat | 4375 ppmv | 14.46° | 18.67° | 291 | 449 | SU_1500 |
| SU_5000-14lat | 5000 ppmv | 14.46° | 24.00° | 291 | 450 | SU_1500 |
| SU_5000-12lat | 5000 ppmv | 11.50° | 14.50° | 297 | 361 | SU_1500 |
| SU_10000-14lat | 10 000 ppmv | 14.46° | 18.65° | 291 | 295 | SU_1500 |

### 5.1.1 Partially Ice-Covered States and Glaciation Bifurcation Point

The temporal evolution of the ice latitude of all simulations started from an ice-free or partially ice-covered state are depicted in Figure 5.1. To begin with, the position of the glaciation bifurcation point can be determined. After that, the evolution of the ice edge allows one to quantify the influence of the ice-albedo feedback on the climate dynamics.

With decreasing $CO_2$ content, the stable ice edge decreases. The ice edge is assumed to be stable if there are no noticeable trends in the position of the ice edge over a time period of 30 years. While the SU_2250 simulation reaches stability at a latitude of 57°, the SU_1875 simulation shows a stable ice edge at 53°. This continues until the SU_1500 simulation, which does not reach a stable ice edge in the mid-latitudes, but instead the sea ice continues to advance towards the equator until a Snowball Earth is reached after 300 years. Thus one can conclude that the deglaciation bifurcation point, at which the stable partially ice-covered states disappear, lies between 1500 ppmv and the simulation with the next higher $CO_2$ content of 1594 ppmv, which resulted in a stable ice edge. Furthermore, the highest possible ice cover of a partially ice-covered state has to have its ice edge at 50° or closer to the equator.

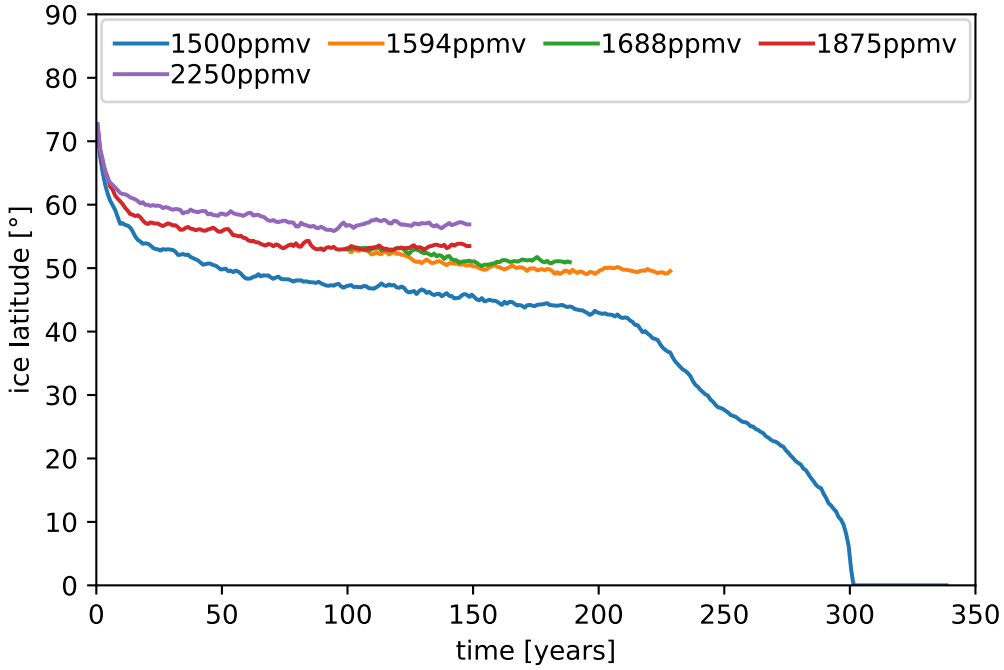


Figure 5.1: Annual mean ice latitude as a function of time for all Semtner-unlimited simulations started from an ice free or partially ice-covered state. The two simulations started from a partially ice-covered state use a restart file out of the SU_1875 simulation (Table 5.1).

All simulations started from an ice-free Earth show rapid growth of ice in the first years, which decreases to a slower growth in the years thereafter. This is partly due to trigonometry, because ice growing from the poles has a strong impact on the value of the sea-ice edge (cf. Equation 4.30). A second reason is the strong instability, i.e., the strong sea-ice albedo effect leading to a rapid loss of energy and thus rapid ice growth. In later years, as the ice edge grows closer towards its stable latitude, the velocity decreases, as the systems becomes less and less unstable. This is particularly visible in the SU_1500 simulation: The ice growth slows down in the mid-latitudes but never reaches stability. After 210 years, the ice edge rapidly accelerates towards the equator. So in the vicinity of the stable partially ice-covered states, the ice growth slows down, but accelerates again with the system reaching more unstable conditions. The acceleration becomes particularly visible in the tropics: It takes only 20 years for the last 20° to freeze over. On reason for this is the increasing influence of the sea-ice albedo effect, as the ice reaches the tropics with accordingly higher values of incoming solar radiation. The higher albedo of the sea ice thus has a particularly strong effect on the global energy budget if sea ice exists in the tropics. Another factor that amplifies this acceleration can be the sea-surface temperatures of the tropical ocean, which cooled down constantly in the previous years and ultimately allow for rapid freezing of the ocean.

### 5.1.2 Separatrix and Jormungand State

The ice latitude of all simulations started from a Jormungand-like state is depicted in Figure 5.2. The direction in which the sea-ice edge changes gives insight into the position of the separatrix: if the ice is growing towards the equator, the separatrix has to be at a higher latitude and vice versa

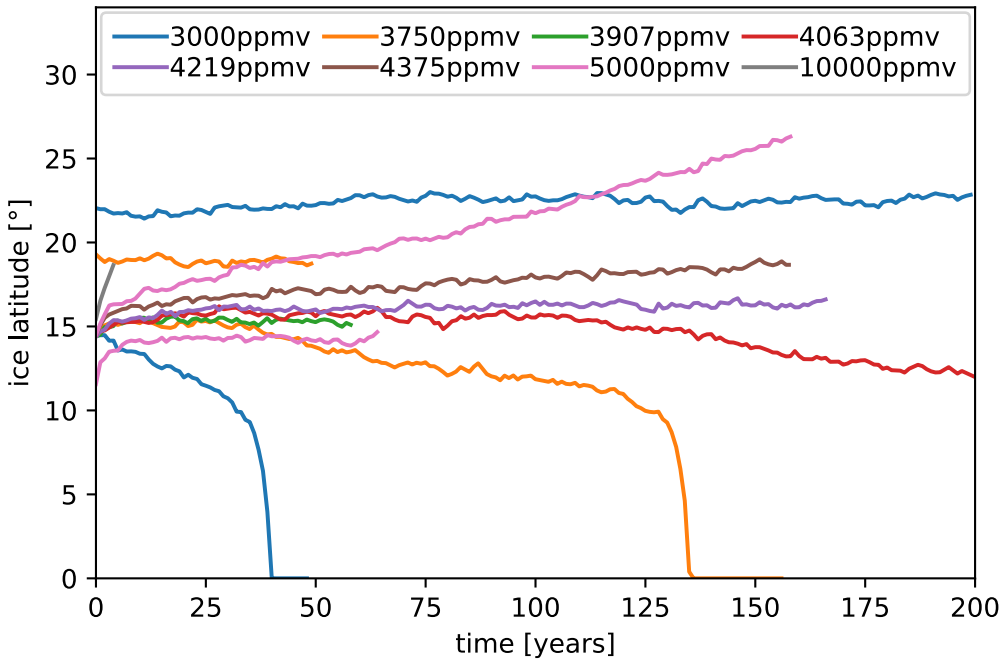


Figure 5.2: Annual mean ice latitude as a function of time for all Semtner-unlimited simulations started from a Jormungand-like state. Simulations starting at $\sim 15°$ and $\sim 11°$ use a restart file out of the 1500 ppmv simulation, the other two a restart file out of the 5000 ppmv simulation (Table 5.1).

(cf. Section 2.2). If the ice edge does not show a clear trend in one direction, two effects could be responsible: Firstly, the system could be in a stable Jormungand state. Secondly, the system could be metastable in the vicinity of the separatrix, meaning that the simulations only appears stable because the simulated period is too short, and given more time, the ice edge would develop in one clear direction. However, a distinction between these two cases (i.e., finding out what time period is long enough to determine the stability of this simulation) would require an in depth analysis of the global energy budget and the atmospheric processes stabilizing or destabilizing the Jormungand state, which is beyond the scope of this thesis.

In Figure 5.2, the ice edge in simulations started from 14° moves in different directions. With lower $CO_2$ content, they drift towards a Snowball Earth (after 32 years for the SU_3000-14lat simulation, after 125 years for the SU_3750-14lat simulation, and slowly drifting towards a Snowball Earth for the SU_3907-14lat and SU_4063-14lat simulations). With a higher $CO_2$ content, they ice edge of the simulations moves towards an ice free state. Conclusively, the position of the separatrix at the latitude of 14° has to be between the two closest simulations that evolved into different directions, which is between 4063 ppmv and 4375 ppmv.

The simulations SU_3000-22lat, SU_3750-19lat, SU_4219-14lat and SU_5000-12lat don't show a clear trend in their ice edge, so they are either in a Jormungand state or a metastable state near the separatrix.

A lot of simulations show rapid increase in the ice latitude in the first 10 years (i.e., the sea-ice edge is retreating in the first years), even when they ultimately grow towards a Snowball Earth

(e.g. SU_3750-14lat). This can be attributed to the fact that these simulations use a restart file from another simulation with a lower $CO_2$ content of 1500 ppmv (Table 5.1). The sudden jump in radiative forcing due to the increase of atmospheric $CO_2$ content after the start of the new simulations likely leads to an initial melting of ice until the atmosphere adapts to the new external forcing.

This Section 5.1 has mapped out the the bifurcation point of glaciation and the position of the separatrix of the Semtner-unlimited simulations in the Snowball Earth bifurcation diagram. This diagram is visualized in Section 5.3, after the comparison with the Semtner-limited simulations in the following Section 5.2.

## 5.2 Comparison: Semtner-unlimited and Semtner-limited

To show the effect of the removal of the sea-ice thickness limitation, the simulations with the same $CO_2$ content (1500 ppmv) of Semtner-unlimited and Semtner-limited are compared in Figure 5.3. Here, an extreme difference between the final sea-ice latitudes of simulations with the same $CO_2$ content can be seen. While the general trend is similar in the first 50 years, the Semtner-limited simulation shows a slowdown of sea-ice growth in the subsequent years, that ultimately leads to a stable ice latitude at 46.6°. This ice latitude is expected to be in an equilibrium, because no further trend towards a Snowball Earth over the last 30 years is visible. In contrast, the Semtner-unlimited simulation continues to expand steadily towards the equator, accelerates after 210 years

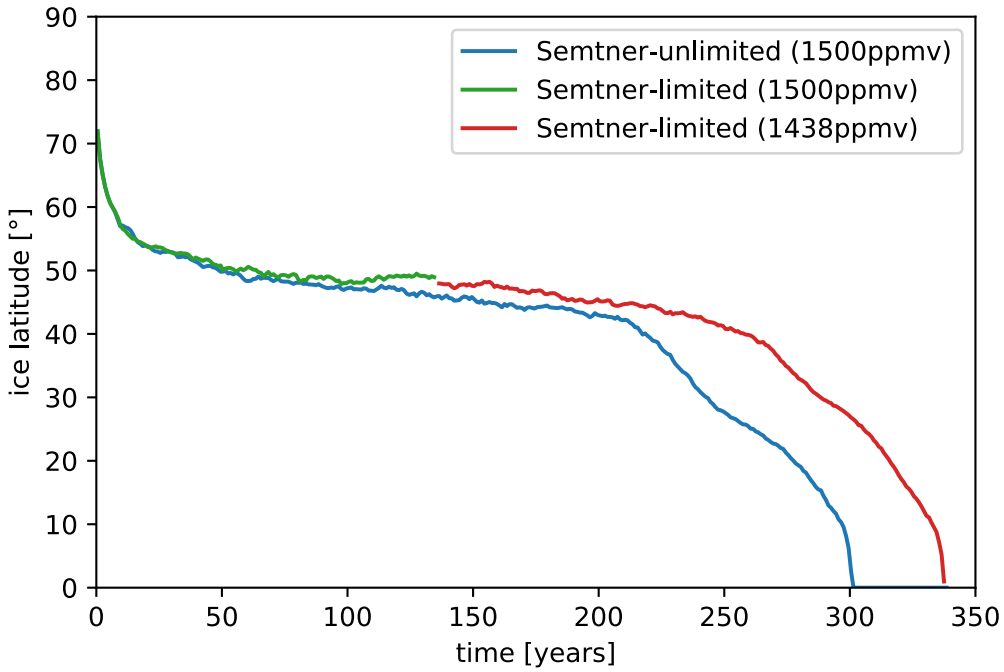


Figure 5.3: Annual mean ice latitude of Semtner-limited and Semtner-unlimited simulations with 1500 ppmv $CO_2$ in green and blue. Additional Semtner-limited simulation with 1438 ppmv in red.

and reaches a Snowball Earth after 300 years. This shows the effect of the sea-ice thickness limitation. Whereas the 1500 ppmv simulation is in a stable partially ice-covered state in Semtner-limited, the removal of the ice thickness limit is enough to push the system over the bifurcation point into a Snowball Earth.

With a decrease of $CO_2$ content to 1438 ppmv in the Semtner-limited simulation (red line in Figure 5.3), the system also ends up being a Snowball Earth. The bifurcation point for the Semtner-limited simulations therefore has to be between 1438 ppmv and 1500 ppmv, whereas for the Semtner-unlimited simulations it is between 1500 ppmv and 1594 ppmv. The bifurcation point is thus pushed towards higher $CO_2$ values with the removal of the ice thickness limit, with the range being between $> 0$ ppmv and $< 156$ ppmv. If the bifurcation point is assumed to be in the middle between each of these two simulations, it would correspond to a shift by $\Delta CO_2 = 78$ ppmv or 5%.

Figure 5.4 shows a Semtner-unlimited and a Semtner-limited simulation started from a Jormungand-like state with an ice edge at roughly 14°, both having a $CO_2$ content of 3000 ppmv. It is clearly visible that the Semtner-unlimited simulation falls into a Snowball Earth much faster, after 40 years, than the Semtner-limited simulation, which requires 165 years. While this does not provide any information about a change in the bifurcation diagram, it shows that the Semtner-limited simulation is more stable than Semtner-unlimited. In other words, the Semtner-unlimited simulation has a much more negative global energy balance than the energy balance of the Semtner-limited simulation, therefore it drifts much faster towards the Snowball Earth. The Semtner-limited simulation may also show faster deglaciation because a smaller amount ice has to be melted at each latitude. However, the impact of this is small, because the thickness difference between Semtner-limited and Semtner-unlimited is only marginal at this latitude range at the start of these simulations. From the ice edge up to 20°, the ice thickness reaches only as high as 2 m at the start of the Semtner-unlimited simulation. The thickness limit of 5 m is only starting to be exceeded at a latitude of 22°. However, the ice of the Semtner-limited simulation still retreats faster in these latitudes.

This indicates the effect of the artificial heat flux resulting from the limitation of sea-ice thickness, which supplies the energy for slowing down the ice growth in the Semtner-limited simulation.

Two similar simulations are depicted in Figure 5.5, both with a $CO_2$ content of 5000 ppmv. In this case, the ice edge in both simulations retreats towards the poles. It does so much faster in the Semtner-limited simulation, reaching an ice edge of 30° after 48 years. The Semtner-unlimited simulation only melted up to an ice edge of 26° after 158 years. This shows again that the Semtner-limited simulation has a more positive energy balance, resulting in faster melting of the ice, further pointing to the existence of an artificial heat flux.

It can be summarized that with an unlimited sea-ice thickness,

1. global glaciation occurs with higher radiative forcing in terms of higher $CO_2$ content.
2. glaciation is faster.
3. deglaciation is slower.

All three effects indicate that the Semtner-limited simulations have an additional heat source in comparison to the Semtner-unlimited simulations. This is the artificial heat flux that results from

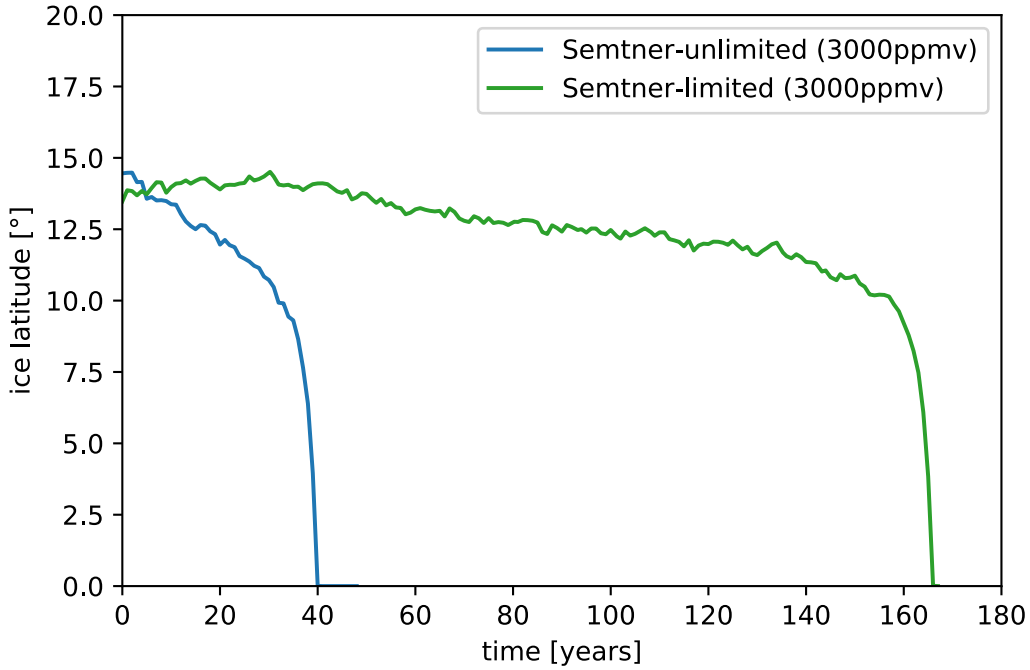


Figure 5.4: Annual mean ice latitude as a function of time for Semtner-limited and Semtner-unlimited simulations with 3000 ppmv, started from a Jormungand-like state.

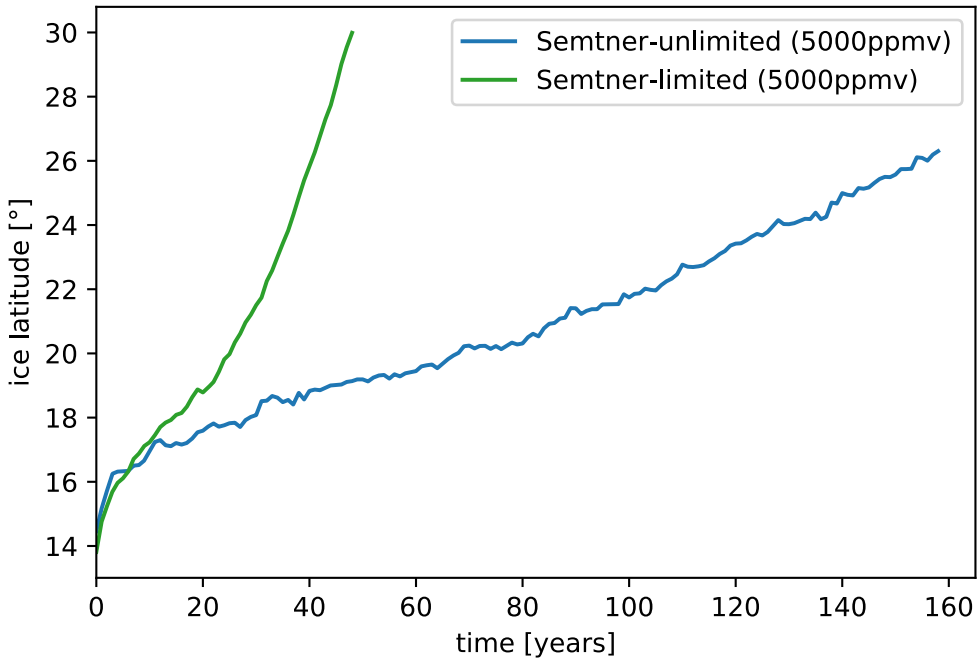


Figure 5.5: Annual mean ice latitude as a function of time for Semtner-limited and Semtner-unlimited simulations with 5000 ppmv, started from a Jormungand-like state.

the limitation of sea-ice thickness in the Semtner-limited simulations. It is described in the following Section 5.2.1.

### 5.2.1 Assessment of Artificial Heat Flux

The artificial heat flux resulting from the limitation of sea-ice thickness is investigated in this section. First, the method used for the calculation of this heat flux is described. Secondly, the resulting heat flux for selected Semtner-limited simulations is investigated.

#### Method of Calculation

When the sea-ice thickness limit is reached, any ice that grows further is removed, resulting in an artificially thin ice layer in the next step and therefore also an artificially high heat flux into the atmosphere. This heat flux corresponds to the amount of latent energy that is released by the formation of the artificially removed ice thickness $\Delta h_{I,rem}$ over the duration of one model time step $\Delta t$.
The removed sea-ice thickness $\Delta h_{I,rem}$ during the output interval $\Delta t_{out}$ is calculated as follows:

$$\Delta h_{I,rem} = \max\left(h_I + \frac{\Delta h_I}{\Delta t}\Delta t_{out} - h_{I,max}, 0\right) \tag{5.1}$$

with the mean sea-ice thickness tendency $\frac{\Delta h_I}{\Delta t}$ integrated over the output interval $\Delta t_{out}$, the mean ice thickness $h_I$ and the ice thickness limit $h_{I,max} = 5\,\mathrm{m}$.
The energy that was released into the atmosphere by the formation of this sea ice can be obtained by using Equation 4.7, which describes the bottom growth of the ice layer without geothermal heat flux as:

$$\frac{\Delta h_I}{\Delta t} = \frac{F_S}{L\rho_I}. \tag{5.2}$$

The sea-ice thickness growth during one time step $\frac{\Delta h_I}{\Delta t}$ is now substituted with the removed ice thickness during the output interval $\frac{\Delta h_{I,rem}}{\Delta t_{out}}$. The artificial heat flux that is released into the atmosphere by the formation of the ice, that is removed afterwards, can thus be defined as:

$$F_{ar} = \frac{L\rho_I \Delta h_{I,rem}}{\Delta t_{out}}. \tag{5.3}$$

The artificial heat flux grows with growing temperature difference between ocean and ice surface. This is because the removed sea-ice thickness $\Delta h_{I,rem}$ is larger if the bottom sea-ice growth $\frac{\Delta h_I}{\Delta t}$ is larger (Equation 5.1). The bottom sea-ice growth $\frac{\Delta h_I}{\Delta t}$ depends on the flux trough the ice $F_S$ (Equation 5.2), which then only depends on the temperature difference between ocean and ice surface temperature, if ice thickness and therefore also snow thickness is limited (Equation 4.1).

#### Artificial Heat Flux in Semtner-limited Simulations

For four Semtner-limited simulations, the amount of latent heat released by the removal of ice thicker the thickness limit is calculated (Fig. 5.6). A clear dependency between ice latitude and the global artificial heat flux is visible. With the sea ice starting to advance from the poles towards the

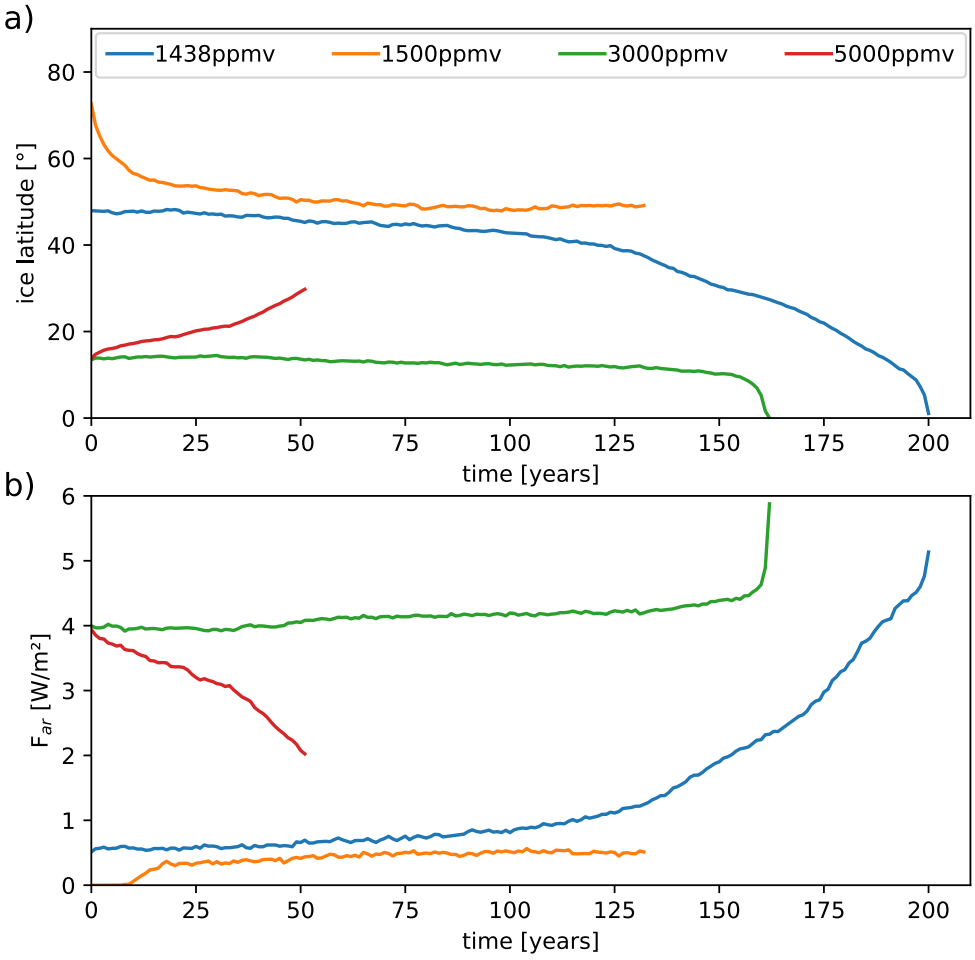


Figure 5.6: a) Annual mean ice latitude as a function of time for Semtner-limited simulations with 1438 ppmv, 1500 ppmv, 3000 ppmv and 5000 ppmv $CO_2$. b) Global mean of the artificial heat flux resulting from the sea-ice thickness limitation in these simulations, calculated using Equation 5.3.

equator in the 1500 ppmv simulation, the heat flux is $0\,\mathrm{W\,m^{-2}}$ initially until the sea-ice thickness limit of 5 m is reached at one point (due to the method of calculation of the artificial heat flux). It reaches a value of $0.5\,\mathrm{W\,m^{-2}}$ at its stable ice latitude of 46.6°. As $CO_2$ content is reduced to 1438 ppmv and ice continues to spread towards the equator, the heat flux increases accordingly, up to a value of $5.1\,\mathrm{W\,m^{-2}}$ in the final Snowball Earth. The heat flux increases with decreasing sea-ice latitude.

The two simulations started from a Jormungand-like state show the same relation. The 3000 ppmv simulation shows a slowly advancing sea-ice edge and a correspondingly increasing artificial heat flux, that reaches up to $5.9\,\mathrm{W\,m^{-2}}$ in a Snowball Earth. In the thawing 5000 ppmv simulation, the artificial heat flux decreases from $3.9\,\mathrm{W\,m^{-2}}$ at the initial sea-ice edge of 13.2° to $2.0\,\mathrm{W\,m^{-2}}$ at 30.3°.

The dependency is summarized by the scatter plot of ice latitude and artificial heat flux in Figure 5.7. Here, a steady growth of the heat flux with growing sea-ice cover is visible. For ice latitudes at the poles, the heat flux is non-existent, due to the fact that no ice has reached its thickness limit yet. The heat flux starts to appear when the ice latitude exceeds 60°, from where on it grows steadily. This can be explained by two factors: Firstly, there is a geometrical reason: with a growing area of sea ice at its thickness limit, this heat flux increases. Secondly, with growing ice sheets and decreasing global temperatures, the temperature gradient between ocean and atmosphere increases, which leads to an increasing artificial heat flux through the ice at any grid point. When complete glaciation is reached, the heat flux increases substantially, which can be explained by the rapidly falling temperatures when reaching a Snowball Earth.

Additionally, the artificial heat flux is converted into an equivalent $CO_2$ content increase, that would be required to provide the same heat flux by an increase of radiative forcing. For this assessment, the equivalent $CO_2$ increase is calculated following Myhre et al. (1998):

$$\mathrm{dCO_2} = \frac{\mathrm{CO_2}}{\mathrm{CO_{2,0}}} = \exp\left(\frac{F_{ar}}{5.35}\right), \tag{5.4}$$

with $CO_{2,0}$ being the original content and $CO_2$ the content that would be required to increase the radiative forcing by the heat flux of $F_{ar}$.

For the 1500 ppmv simulation, the simulation with the lowest $CO_2$ content closest to the bifurcation point, it reaches a value up to 0.5 $\mathrm{W\,m^{-2}}$ and an equivalent $CO_2$ content increase of 10% at the final ice latitude of 46.6° (see Fig. 5.7). Idealized, this means that a 10% higher $CO_2$

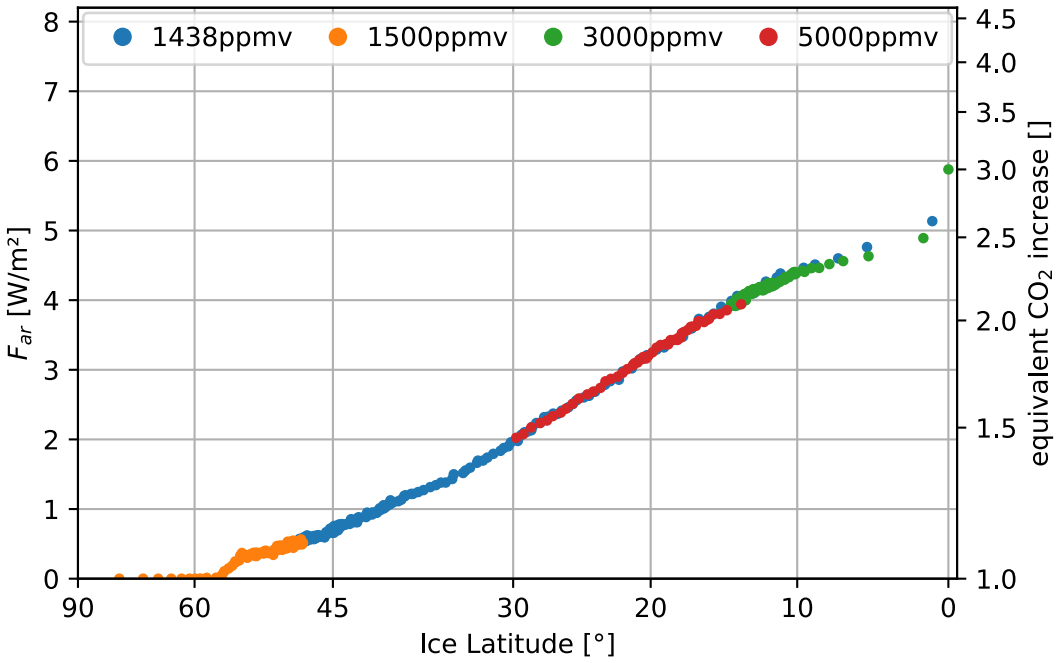


Figure 5.7: Scatter plot of annual mean artificial heat flux and ice latitude in selected Semtner-limited simulations. On the second y-axis, the equivalent $CO_2$ content increase required to provide the same heat flux is depicted, assessed according to Myhre et al. (1998).

content (1650 ppmv) is required to provide the same external forcing of the atmosphere using the Semtner-unlimited model. According to this assessment, the bifurcation diagram at this point should be shifted to higher values by 10% or 150 ppmv. This estimated increase has the same magnitude as the observed shift of 5%. Additionally, when the sea-ice cover is growing towards a Snowball Earth, the heat flux and the equivalent $CO_2$ content is rising significantly, up to an equivalent $CO_2$ increase of 200% or a factor of 3 (see Fig. 5.7).

However, it should be noted that this is a highly idealized assessment, because it assumes that heating of the atmosphere from the bottom is equivalent to heating from above by well-mixed greenhouse gases.

In summary, the artificial heat flux heats the atmosphere in the Semtner-limited simulations. It has no impact at all if the ice thickness limit is not reached, but an increasing impact if the sea-ice cover grows and global surface temperatures fall. For the bifurcation diagram, this means that it is pushed towards higher $CO_2$ values in the Semtner-unlimited simulations, with an increasing difference at lower ice latitudes, due to the higher heat flux and therefore also higher equivalent $CO_2$ increase.

## 5.3 Summary: Effects on the Bifurcation Diagram

The influence of the artificial heat flux arising from the limitation of sea-ice thickness can be summarized in the bifurcation diagram of the Semtner-limited and Semtner-unlimited simulations. In Figure 5.8, the $CO_2$ content and sea-ice latitude of all Semtner-limited (a) and Semtner-unlimited (b) simulations are depicted. From the sea-ice latitude at the end of every simulation, the estimate of the bifurcation diagram is constructed. The $CO_2$ content on the x-axis is in a logarithmic scale, due to the logarithmic influence of $CO_2$ on radiative forcing (Myhre et al., 1998).

It can be seen that in the Semtner-unlimited simulations, the bifurcation diagram is moved towards higher $CO_2$ levels. This becomes especially visible at the bifurcation point of glaciation, where the Semtner-unlimited simulation with 1500 ppmv $CO_2$ falls into a Snowball Earth, while the Semtner-limited simulation stays stable at a partially ice-covered state. The bifurcation point of glaciation is pushed towards higher $CO_2$ values in the Semtner-unlimited simulation, by an amount of $\Delta CO_2 = 78$ ppmv or a relative increase of 5%, as described in detail in Section 5.1.1.

The position of the separatrix at lower ice latitudes is more difficult to estimate accurately, as described in Section 5.1.2. While the simulations with a clear trend in sea-ice edge allow a clear estimation of the position of the separatrix, the four metastable states just show that they are likely to be close to the the separatrix. The exact position of the separatrix should therefore be seen with caution, and more as an indicator of the region where the separatrix actually lies.

However, a shift towards higher $CO_2$ values in the Semtner-unlimited simulations can still be seen. Especially the Semtner-limited simulations at 3000 ppmv and the Semtner-unlimited simulations around 4000 ppmv show this: In Semtner-limited, the separatrix at $\sim 14°$ is at a $CO_2$ content of $\sim 3000$ ppmv. In Semtner-unlimited, the separatrix at the same latitude has a $CO_2$ content of $\sim 4200$ ppmv. This is additionally supported by the fact that the Semtner-unlimited simulations started from ice edges at lower latitudes reach a Snowball Earth much faster than the Semtner-limited simulations (Section 5.1), showing that they are further away from the separatrix.

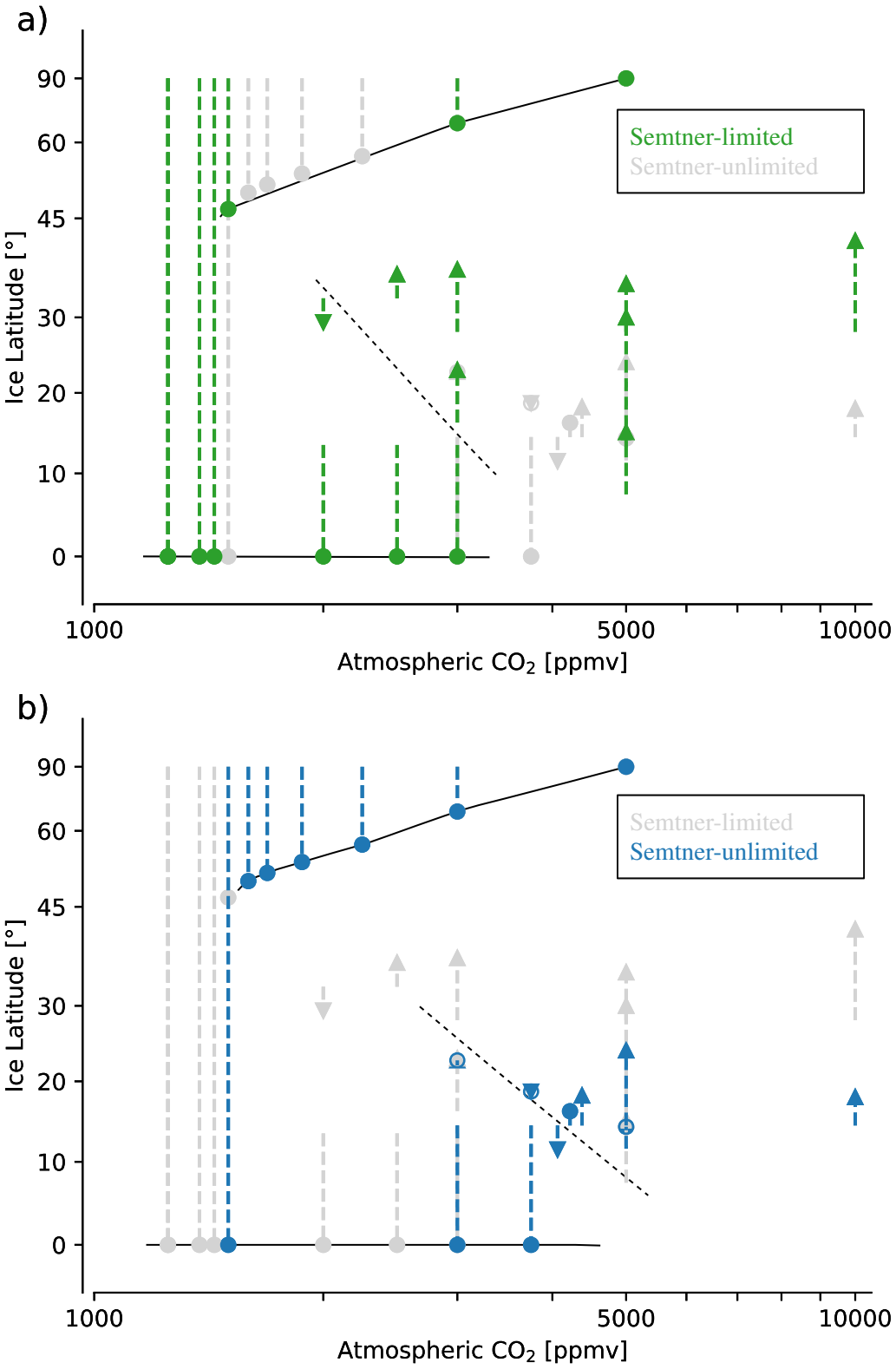


Figure 5.8: Bifurcation diagram of a) Semtner-limited simulations in green, with estimated position of stable states in solid black and of the separatrix in dashed black, The Semtner-unlimited simulations are shown in grey for reference. b) Semtner-unlimited simulations in blue, and Semtner-limited simulations shown in grey for reference. A filled (empty) circle indicates a stable (metastable) end state, an arrow indicates a continuous trend in the sea-ice edge.

It can be concluded that the artificial heat flux resulting from the limited sea-ice thickness in the Semtner-limited simulation leads to a shift in the bifurcation diagram towards lower $CO_2$ values in comparison to the Semtner-unlimited simulations. This shift becomes stronger when the sea-ice edge is at lower latitudes, as the magnitude of the artificial heat flux is higher with a larger sea-ice cover and colder temperatures. The assessment of the artificial heat flux in the previous section indicates a shift to a 10% higher $CO_2$ content at the bifurcation point, increasing up to a 200% increase in a Snowball Earth. This confirms that the artificial heat flux is in fact responsible for the observed shift in the bifurcation diagram.

## 5.4 Discussion

To assess the importance of the shown impact of a sea-ice thickness limitation, it has to be set in context to other effects on the bifurcation. Other physical mechanisms associated with sea ice have a much larger impact. Voigt and Abbot (2012) showed that sea-ice dynamics decrease the $CO_2$ necessary for glaciation by a factor of 100, while changes in ice albedo and ocean heat transport change it by a factor of 2. Chapter 6 shows that increasing the vertical resolution increases the $CO_2$ by a factor of 1.5. Removal of the ice-thickness limit however shows a change of $\sim 5\%$, or an increased $CO_2$ content by a factor of 1.05. The impact of a sea-ice limit on the initiation of Snowball Earth is therefore small in comparison to other details of the sea-ice scheme like ice dynamics, ice albedo or ice vertical resolution.

However, this impact increases with increasing sea-ice cover. In a Snowball Earth, the limitation of sea-ice thickness results in a heat flux that accounts for an increase in $CO_2$ by a factor of 3. This factor is even expected to increase further, until the Snowball Earth has reached its final equilibrium temperature.

The importance of an unlimited sea-ice thickness is therefore highly dependent on the area of application in the Snowball Earth cycle. For the investigation of the glaciation bifurcation point, there is no substantial effect. For investigations of Snowball Earth deglaciation or the stability of near-snowball states however, the importance of using an unlimited sea-ice thickness increases, because the artificial heating of the atmosphere increases. Additionally, the extremely thin ice cover at the equator would lead to a further underestimation of the $CO_2$ content required for deglaciation, because the thin ice is much easier to melt.

Generally it can be concluded that the limitation of sea-ice thickness should be avoided if possible, simply because it is not physically correct. This is especially the case when a limitation is not a numerical necessity, for example because a mixed-layer ocean is used. While the impact is negligibly small for Snowball Earth initiation, it becomes increasingly important when a Snowball Earth or near-snowball state is reached.

# 6 Impact of Increased Vertical Resolution

In this Chapter, the impact of increased vertical resolution of the sea-ice scheme on Snowball Earth initiation is investigated. For this, multiple simulations using the 3-layer Winton sea-ice model (Section 4.1.2) are carried out, whose details are listed in Table 6.1.
To begin with, an overview of all Winton simulations is given in Section 6.1. The focus is on the transition from an ice-free state into a Snowball Earth, the development of the sea-ice edge and the implications on the bifurcation diagram.
In Section 6.2, the bifurcation diagram of the Winton simulations is investigated and compared with the bifurcation diagram of the Semtner-unlimited simulations (cf. Section 5.3). The observed differences in these bifurcation diagrams are then investigated in detail in the following subsections, by applying offline ice-models with idealized boundary conditions, by investigating the diurnal processes at the ice border and by studying the effects on global ice growth and albedo. Finally, Section 6.3 summarizes the results and Section 6.4 puts them into context.

## 6.1 Evolution of the Sea-Ice Edge

### 6.1.1 Partially Ice-Covered States and Glaciation Bifurcation Point

The development of the ice edge of all Winton simulations that were started from an ice-free or partially ice-covered state is depicted in Figure 6.1. The direction in which the ice edge develops for simulations with a certain $CO_2$ content allows for the determination of the position of the bifurcation point.
All simulations except one show sea-ice growth towards the equator as time progresses. For the simulations W_2437, W_2625 and W_3000, this results in a stable ice edge in the mid-latitudes, with the position of the ice edge being at lower latitudes with decreasing $CO_2$ content. These simulations show the existence of partially ice-covered states in this range of atmospheric $CO_2$ content.
The W_5000 simulation is the only one that does not show any sea-ice cover after a certain spin-up time period. For this $CO_2$ content, Earth is thus in a completely ice-free state.
The W_1875 W_2250 simulations however show a growing sea-ice cover until a Snowball Earth is reached. The $CO_2$ content of these simulations therefore has to be below the bifurcation point. The bifurcation point therefore has to have a $CO_2$ content between 2250 ppmv, the simulation with the highest $CO_2$ content resulting in a Snowball Earth, and 2375 ppmv, the simulation with the lowest $CO_2$ content resulting in a partially ice-covered Earth. Additionally, the furthest ice extent of a stable partially ice-covered state, i.e., the position of the bifurcation point in terms of latitude, thus has to be at $\leq 50.5°$.

Table 6.1: List of all Winton simulations performed. The $CO_2$ content is constant throughout the simulation. Start and end ice latitude refers to the latitude of the sea-ice edge at the start and end of the simulation, 90° being ice free and 0° a Snowball Earth. When the start year is larger than 1, the simulation was started from a restart file from that year of another simulation, listed in the initial conditions. Otherwise it was started from ice-free initial conditions (cf. Section 4.2.1).

| simulation name | $CO_2$ content | start ice latitude | end ice latitude | start year | start year | initial conditions |
|---|---|---|---|---|---|---|
| W_1875 | 1875 ppmv | 90° | 0° | 1 | 100 | aqua-icefree |
| W_2250 | 2250 ppmv | 90° | 0° | 1 | 200 | aqua-icefree |
| W_2437 | 2437 ppmv | 58.9° | 50.5° | 50 | 200 | W_3000 |
| W_2625 | 2625 ppmv | 58.9° | 52.6° | 50 | 200 | W_3000 |
| W_3000 | 3000 ppmv | 90° | 56.3° | 1 | 130 | aqua-icefree |
| W_3000-30lat | 3000 ppmv | 30.2° | 0° | 80 | 130 | W_1875 |
| W_3000-15lat | 3000 ppmv | 15.3° | 0° | 92 | 120 | W_1875 |
| W_4219-30lat | 4219 ppmv | 30.2° | 0° | 80 | 130 | W_1875 |
| W_4219-17lat-SR | 4219 ppmv | 16.6° | 0° | 457 | 480 | SU_4219-14lat |
| W_5000 | 5000 ppmv | 90° | 90° | 1 | 30 | aqua-icefree |
| W_5000-39lat | 5000 ppmv | 38.9° | 54.3° | 70 | 100 | W_1875 |
| W_5000-15lat | 5000 ppmv | 15.3° | 0° | 92 | 130 | W_1875 |
| W_5000-15lat-SR | 5000 ppmv | 14.5° | 0° | 291 | 330 | SU_1500 |
| W_10000-15lat | 10 000 ppmv | 15.3° | 6° | 92 | 102 | W_1875 |

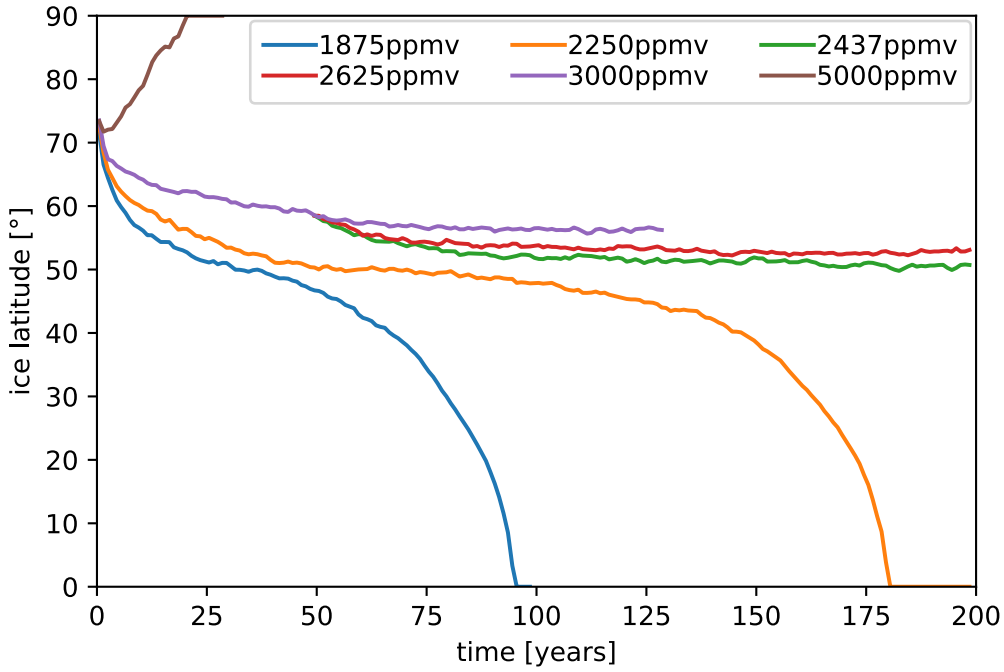


Figure 6.1: Annual-mean ice latitude as a function of time for all Winton simulations started from an ice free or partially ice-covered state. The two simulations started from a partially ice-covered state at 59° use a restart file out of the W_3000 simulation (Table 6.1).

The process of glaciation shows the same characteristics as in the Semtner simulations described in Section 5.1. The W_2250 simulation shows a slowdown of sea-ice growth in the mid-latitudes in the vicinity of stable partially ice-covered states and subsequent acceleration after an ice edge of $\approx 50°$ is surpassed after $\approx 100$ years. The W_1875 shows only a brief slowdown in the mid-latitudes, after 30 years the ice edge surpasses 50° and the ice growth accelerates again. This rapid ice growth and the corresponding brief slowdown indicates the strong instability resulting from a strong ice-albedo feedback due to a $CO_2$ content much lower than that of the bifurcation point.
Compared with the development of the sea-ice edge of the Semtner simulations in Section 5.1, it is noticeable that the $CO_2$ content required to achieve either a stable partially ice-covered state or a retreating ice edge is higher using the Winton model than using the Semtner model. This observation is further detailed in the bifurcation diagram in Section 6.2.

### 6.1.2 Separatrix and Jormungand State

All Winton simulations started from a Jormungand-like state are depicted in Figure 6.2. These simulations are started from different ice latitudes (cf. Table 6.1), with the goal of obtaining both simulations with a growing sea-ice cover as well as simulations with a retreating sea-ice cover, i.e., simulations that are below and above the separatrix.
In contrast to the Semtner-unlimited simulations described in Section 5.1, no metastable states are visible. Instead, all simulations show instability. All simulations except one show a rapidly growing sea-ice cover that ultimately results in a Snowball Earth. Notable is the W_10000 simulation, which still shows a growing sea-ice cover in spite of the high amount of $CO_2$. The starting point of all these simulations therefore has to be below the separatrix.

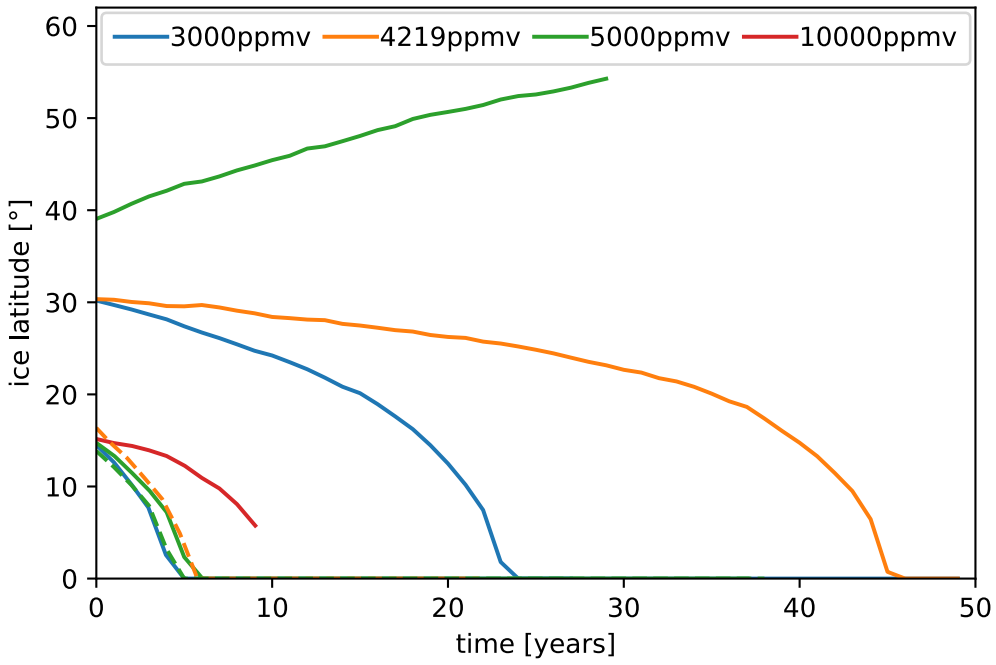


Figure 6.2: Annual-mean ice latitude as a function of time for all Winton simulations started with an ice-edge at lower latitudes close to the separatrix. The restarts used are listed in Table 6.1.

The only simulation showing a retreating ice border, i.e., the only simulation that has been started above the separatrix, is the one started from an ice edge at 39° with an atmospheric $CO_2$ content of 5000 ppmv.

### Impact of Initial Ice Temperature

Using the Winton sea-ice model, the heat capacity of the ice is an additional factor that could potentially increase the inertia of the climate system and thus increase the importance of initial conditions. If a restart file from a simulation showing extremely fast ice growth is used, the low internal ice temperatures could potentially enhance the ice growth at the beginning of the simulation using this restart file.

It has been shown that this is not the case, by performing the W_5000-15lat-SR simulation with 5000 ppmv $CO_2$ using a Semtner-unlimited restart file with an ice edge at $\sim 15°$. This has the effect that the internal ice temperatures are at a default value of $-1.9\,°C$. The internal ice temperatures of the simulation using a Winton restart file has much lower ice temperatures, but the same initial ice edge and $CO_2$ content.

In Figure 6.2 it is visible that both simulations (dashed green and solid green) show an almost identical evolution of their ice edge, indicating that the impact of the initial internal ice temperature on the development of the ice edge is negligibly small.

## 6.2 Comparison: Winton and Semtner

In this section, the impact of the increased vertical ice resolution is analyzed by comparing the simulations using the 3-layer Winton model with those using the 0-layer Semtner-unlimited model. The Semtner-unlimited simulations are used as a comparison, because they do not result in an artificial heat flux (cf. Chapter 5).

To show the differences in these simulations, the development of the ice latitude of three simulations are compared. The Winton simulation with the highest $CO_2$ content of 2250 ppmv that developed into a Snowball Earth is compared with the Semtner-unlimited simulation having the same $CO_2$ content in Figure 6.3.

The striking difference between the Winton and Semtner-unlimited simulation is the fact that while the Winton simulation ends up in a Snowball Earth with 2250 ppmv $CO_2$, the Semtner-unlimited simulation with the same $CO_2$ content stays stable with the ice edge being at $\sim 57°$. Additionally, Semtner-unlimited requires a $CO_2$ content as low as 1500 ppmv for global glaciation to occur. While the development of the ice latitude is similar in the first 100 years, the ice growth in Winton accelerates after that. The Semtner-unlimited simulation however takes more than 100 years longer for global glaciation to occur.

Ultimately, this comparison provides one example for the Winton model leading to faster glaciation as well as glaciation in spite of higher radiative forcing in comparison to the Semtner-unlimited model. This indicates that using the Winton model leads to a stronger ice-albedo feedback resulting in enhanced glaciation.

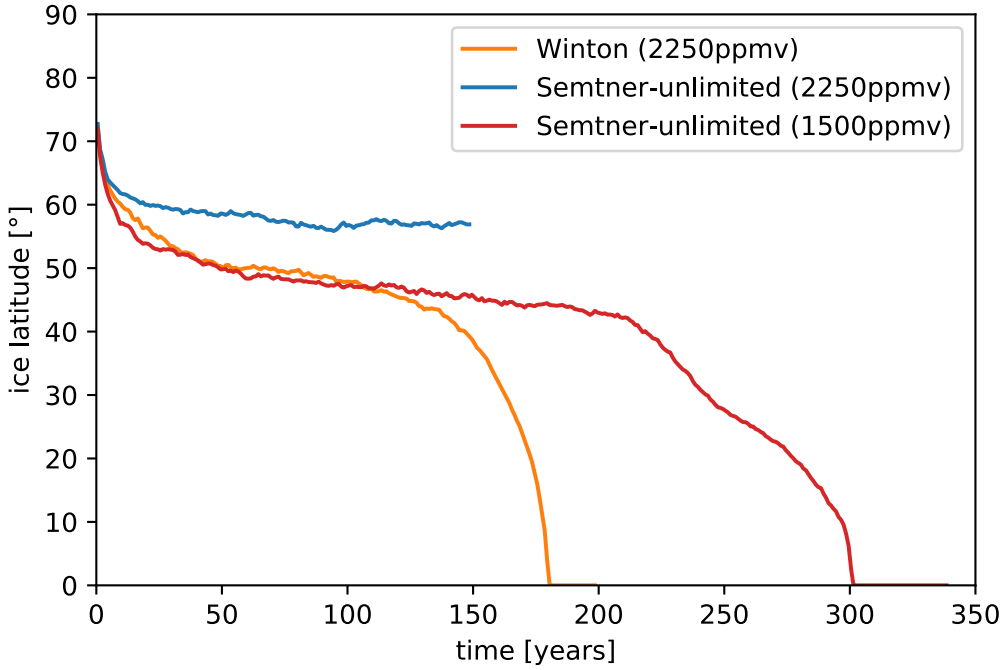


Figure 6.3: Annual-mean ice latitude as a function of time for Winton (orange) and Semtner-unlimited (blue) simulations with 2250 ppmv $CO_2$. An additional Semtner-unlimited simulation with 1500 ppmv is shown in red.

### 6.2.1 Effects on the Bifurcation Diagram

To summarize the observed differences between the simulations using the different sea-ice schemes, all start and end points of the Winton and Semtner-unlimited simulations are depicted in the bifurcation diagram in Figure 6.4.

At an ice-free state with 5000 ppmv atmospheric $CO_2$ content, there are no differences in the bifurcation. At this point, there is practically no sea ice present and thus the different sea-ice schemes have no impact. However the difference increases with increasing sea-ice cover.

The next simulations with the same $CO_2$ content of 3000 ppmv show that the Winton simulations results in a larger sea-ice cover up to 56° latitude, while Semtner-unlimited simulations result in a stable ice edge at 65°. Correspondingly, simulations resulting in a comparable ice edge have a higher $CO_2$ content using the Winton model. This is most visible at the glaciation bifurcation point: In Semtner-unlimited simulations (Fig. 6.4 a), the partially ice-covered state with the lowest $CO_2$ content is at 1594 ppmv with an ice edge at $\sim 50°$. In Winton simulations (Fig. 6.4 b) however, it is the simulation with 2437 ppmv $CO_2$ that still shows stability with a partial sea-ice cover at $\sim 51°$. The glaciation bifurcation point is thus pushed towards higher $CO_2$ values by between 656 ppmv and 937 ppmv atmospheric $CO_2$ when the Winton instead of the Semtner model is used. Assuming the position of each bifurcation point to be in the middle between these two simulations, the difference is $\Delta CO_2 = 797$ ppmv. In relative terms, Winton simulations require a 52% higher $CO_2$ content than Semtner-unlimited simulations for glaciation to start. The differences in the stable partially ice-covered states therefore indicate a stronger ice-albedo feedback in the Winton model.

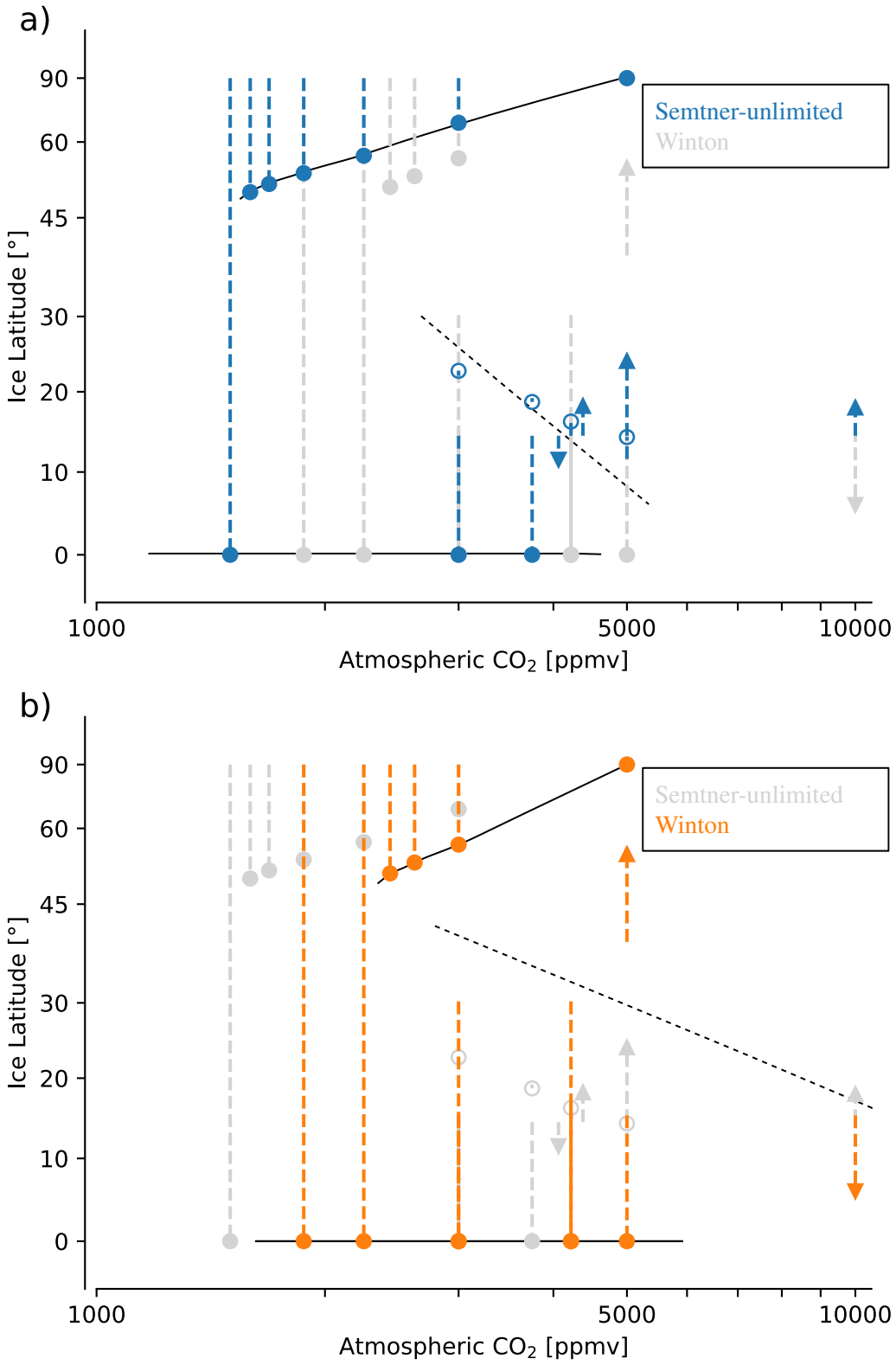


Figure 6.4: Bifurcation diagram of a) Semtner-unlimited simulations in blue, with estimated position of stable states in solid black and of the separatrix in dashed black, The Winton simulations are shown in grey for reference. b) Winton simulations in orange, and Semtner-unlimited simulations shown in grey for reference. A filled (empty) circle indicates a stable (metastable) end state, an arrow indicates a continuous trend in the sea-ice edge.

Looking at the position of the separatrix, the same effect is visible. Simulations that showed a metastable ice edge or developed into an ice-free state in Semtner-unlimited all end up in a Snowball Earth in the Winton simulations, although they are started from the same ice edge (3000 ppmv, 4219 ppmv, 5000 ppmv and 10 000 ppmv). Even if started from a even smaller sea-ice cover at 30°, Winton simulations still form a Snowball Earth (3000 ppmv and 4219 ppmv). The only simulation that has been found to show a decreasing global sea-ice cover using the Winton model is with 5000 ppmv started from an ice edge as high as $\sim 39°$. This again shows the enhanced sea-ice albedo feedback in the Winton model: even for a smaller sea-ice cover, these simulations reach a negative global energy balance that results in global glaciation. The separatrix is thus pushed towards both higher $CO_2$ values and higher ice latitudes.

### 6.2.2 Ice-Physics Investigation Using Offline Ice Models with Idealized Boundary Conditions

It is difficult to accurately compare the ice physics of the different ice schemes in Snowball Earth simulations using a complex model such as ICON. This is due to the fact that changing the ice schemes impacts the global climate, as has been shown in the previous subsections. Following this, the processes happening at the ice surface are difficult to compare between Semtner-unlimited and Winton, because the atmospheric boundary conditions of the ice, are affected by the change of the sea-ice scheme. For example, simulations that showed a different stable ice edge with the same $CO_2$ content cannot be compared in terms of the processes at the ice surface, because the whole climate is in a different state: the simulation with the ice edge at lower latitudes has a significantly lower global temperature. This is a consequence of the ice-albedo feedback: changing ice physics impacts the global climate which influences ice growth again.

To address this problem, the Semtner 0-level model and the Winton model have been implemented by the author using python to investigate the differences of the model physics in an isolated environment. The details of these models are described in Section 4.3.

To show the melt-ratchet effect and its varying impact in the different ice schemes, both offline models are forced with the same idealized boundary using an oscillating incoming shortwave radiation $S\downarrow = \max\left(-500\cos\left(2\pi t\right)\mathrm{W\,m^{-2}}, 0\right)$ to mimick the diurnal cycle and a constant downward sensible heat flux of $F\downarrow_{sen} = 60\,\mathrm{W\,m^{-2}}$.

It should be kept in mind that these boundaries condition can change radically in a Snowball Earth simulation, as the Earth cools down by developing into a Snowball Earth, showing a much more negative surface energy balance. These specific boundary conditions are therefore only one example to visualize the melt-ratchet effect which would occur at different times on various scales during a Snowball Earth simulation.

The boundary conditions result in melting of ice in both models, as can be seen in Figure 6.5 a). This can mainly be attributed to the large net surface heat flux (Fig. 6.5 b), which leads to surface melting during the day due to the incoming solar radiation. The Semtner model shows a maximum heat flux during noon which is more than $50\,\mathrm{W\,m^{-2}}$ larger than the maximum heat flux of the Winton model. The minimum heat flux during night however is $0\,\mathrm{W\,m^{-2}}$ in both models, due to the fact that surface freezing is not implemented in either model. On average, the Semtner

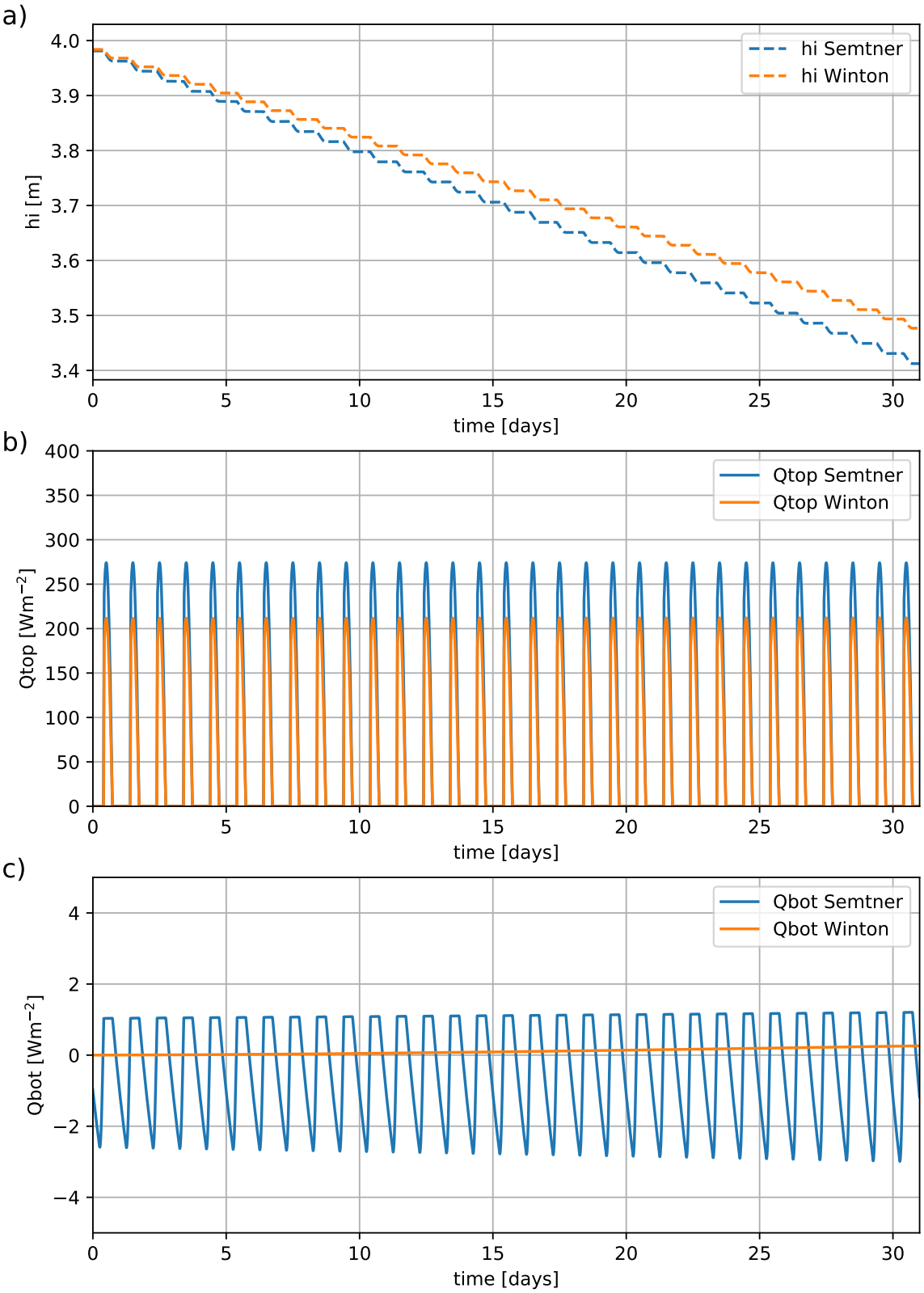


Figure 6.5: Ice thickness (a), heat flux for top melting (b) and heat flux for bottom melting (c) in the offline Semtner and Winton models. Boundary conditions are an oscillating shortwave radiation of $S\downarrow = \max\left(-500\cos\left(2\pi t\right)\mathrm{W\,m^{-2}}, 0\right)$ and a constant sensible heat flux of $F\downarrow_{sen} = 60\,\mathrm{W\,m^{-2}}$. A positive heat flux indicates melting and a negative heat flux indicates freezing.

model shows a heat flux of $65.4\,\mathrm{W\,m^{-2}}$, in contrast to $48.9\,\mathrm{W\,m^{-2}}$ in Winton. The higher vertical resolution therefore decreases top melting by $\sim 25\%$ in this case.

The bottom freezing (Fig. 6.5 c) also shows differences between the two models. While the Winton model shows a small bottom melt which increases slowly from $0\,\mathrm{W\,m^{-2}}$ to $0.2\,\mathrm{W\,m^{-2}}$ due to the continuous warming of the ice, the Semtner model shows a bottom heat flux that oscillates between freezing during night and melting during day, following the diurnal cycle. This comes from the lack of any internal ice temperature in the Semtner model, which means that the bottom heat flux is determined solely by the surface temperature and ice thickness. On average, the Semtner model shows a bottom heat flux of $-0.3\,\mathrm{W\,m^{-2}}$, whereas the Winton model results in a bottom heat flux of $0.1\,\mathrm{W\,m^{-2}}$. The Semtner model thus results in small scale bottom freezing, while the Winton model results in bottom melting. This can be attributed to the warming ice temperatures in Winton, which enhance the melting of ice. However, the magnitude of the bottom heat fluxes is much smaller than that of the top heat fluxes.

In total, the bottom and top heat flux results in net melting, which is stronger in Semtner due to the stronger top heat flux. This indicates that the melt-ratchet effect is stronger in the Semtner model, resulting in faster ice melt/slower ice growth in the Semtner model (Figure 6.5 a). Although the Semtner model shows more freezing during the night, this is not enough to compensate for the increased surface melting. To show that this effect does not only exist for offline sea-ice models in an idealized environment but also takes place in the ICON simulations carried out, the diurnal processes at the ice edge in two Winton and Semtner-unlimited simulations are compared in the next section.

### 6.2.3 Diurnal Processes at the Ice Edge

In this section, data of simulations with higher temporal output resolution of 10 min is investigated to demonstrate the diurnal effects at the ice surface. The simulations investigated are W_3000 and SU_2250, both started from an ice-free state. Both showed a comparable latitude of the stable sea-ice edge at 56.3° and 56.9° (Tables 5.1 and 6.1).

The problem with finding adequate simulations to compare the ice-surface effects of the different ice models lays with finding two simulations that are both in a stable state and have comparable boundary conditions for the ice. Simulations in a Snowball state can't be used, as they haven't been running long enough to reach stability and the Earth has still a negative global energy balance at the time the simulations are stopped. Therefore, simulations in a stable partially ice-covered state are used. The disadvantage of using those is that due to the sea ice only existing in high latitudes, the effect of the diurnal cycle on the sea ice is smaller. From both simulations, high-frequency 10 minute output is analysed for the same 7 days in January.

To compare the effects at the ice surface, an area of the sea-ice edge in the summer hemisphere (southern hemisphere) is selected between 55°S and 60°S, so that the effect of the diurnal cycle is visible in the sea-ice physics. In this regions, all grid points showing an ice thickness larger than 0.05 m over the whole time span are selected and interpolated to local time, so that the diurnal cycle in the zonal mean can be compared. There was no snow cover on any of the grid points.

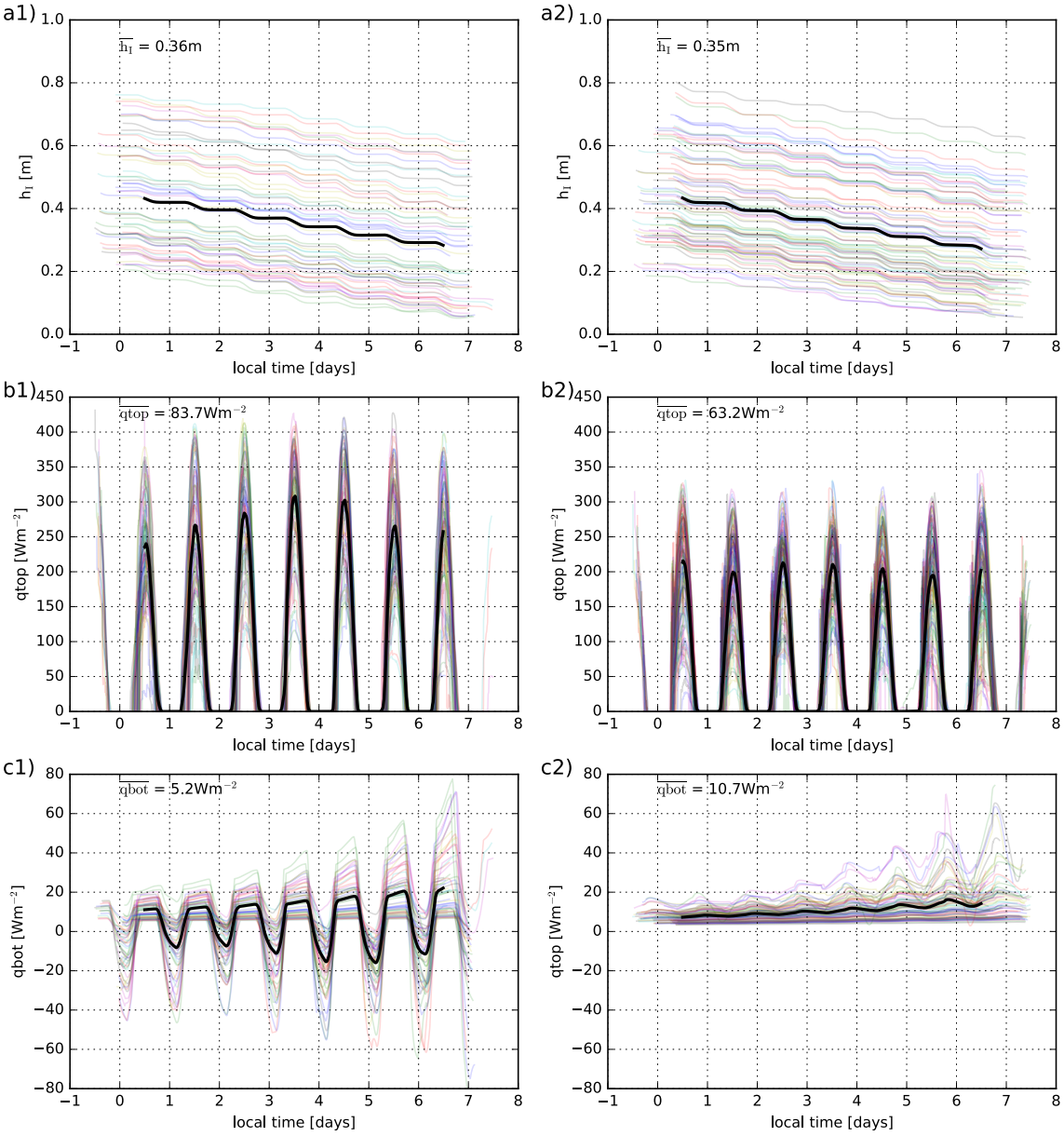


Figure 6.6: Ice thickness (a), heat flux for top melting (b) and heat flux for bottom melting (c) in the Semtner-unlimited (1) and Winton (2) model. The simulations used are W_3000 and SU_2250, with high-frequency 10 minute output for the same 7 days in January. (see Tables 5.1 and 6.1). An area between 55°S and 60°S is considered. The x-axis is in local time, with 0 marking the local midnight for each grid cell. Colored lines indicate the values at individual grid points, black lines the average over all grid points. The represented time period is the first week of January. A positive heat flux indicates melting, a negative heat flux indicates freezing.

The ice thickness and the heat fluxes for top and bottom melting are depicted in Figure 6.6. It can be seen that the ice thickness (Fig. 6.6 a) is very similar in both models. However, the values of the heat fluxes at the top (Fig. 6.6 b) and the bottom (Fig. 6.6 c) of the sea-ice differ substantially. The mean ice thickness (Fig. 6.6 a) in both models decreases from 0.43 m to 0.27 m. Additionally, all grid points show an ice thickness in a comparable range, from 0.2 m to 0.8 m at the start. Ice gradually melts in both models, with the maximum melt during noon and almost no melt during the night. While there are no differences in the net change of sea-ice thickness visible during this week, the differences in top and bottom fluxes are still observable. This is due to the short

simulation period and due to the small incoming radiation in comparison to the offline models in Section 6.2.2. A longer simulation or an investigation of the sea-ice surface in lower latitudes would be required to show a visible difference between the sea-ice thickness of the models.

Looking at the heat flux for top melting (b), the effect of the diurnal cycle is visible in both models: no melting during the night and increasing melting during daytime. This is the melt-ratchet effect as described in Section 2.3. However, the amplitude is larger in the Semtner model, reaching a daily maximum as high as $308\,\mathrm{W\,m^{-2}}$, in comparison to the daily maximum of $215\,\mathrm{W\,m^{-2}}$ in Winton. This can be attributed to the nonexistent heat capacity of the ice in the Semtner model, which leads to larger temperature fluctuations. As no surface freezing can take place to counteract this difference, Semtner results in a higher average surface melting heat flux of $83.7\,\mathrm{W\,m^{-2}}$ in comparison to Winton with $63.2\,\mathrm{W\,m^{-2}}$. This is a decrease of $\sim 25\%$, the same amount as has been shown with idealized boundary conditions in the previous section. The impact of the melt-ratchet effect is thus weaker in the Winton model.

Regarding the bottom heat flux (c), the diurnal cycle is only visible in the Semtner model, showing maximum melting at noon and maximum freezing at night. This is due to the fact that bottom melting is determined by the surface temperature in the Semtner model (cf. Section 4.1.1). In the Winton model, however, there is almost no signal of the diurnal cycle. Melting takes place at all times at all grid points, with only a small variability during day and night. Only grid points with a smaller ice thickness show significant diurnal variability. This can be explained by the internal ice temperatures which determine the bottom growth in the Winton model, dampening the impact of the diurnal cycle (cf. Section 4.1.2). Due to the bottom freezing at night in the Semtner model, the average heat flux of $5.2\,\mathrm{W\,m^{-2}}$ is smaller than in the Winton model with $10.7\,\mathrm{W\,m^{-2}}$, meaning that the Winton model melts more from the bottom than the Semtner model does. The bottom heat flux increases with time in both models, which is a result of the decreasing ice thickness.

The effects of the ice model change on surface and bottom melting are therefore different: Winton leads to decreased top melting but also increased bottom melting. However, the effect on top melting is larger, as can be seen by the magnitudes of the heat fluxes. This is due to the fact that the ice thickness dampens the heat flux through the ice and thus bottom melting, both using the Semtner and the Winton model. The larger the ice thickness, the smaller the bottom heat flux will be in both models. This indicates that the melt-ratchet effect is weakened using the Winton model, resulting in less ice melting at the surface. This is consistent with the results of the previous section, showing that the differences between the Winton and the Semtner model can be shown both in offline models with idealized boundary conditions as well as in the ICON model.

### 6.2.4 Effects on Global-Mean Sea-Ice Growth

In this section, the decreased melt-ratchet effect using the Winton model is shown by analyzing the global-mean values for bottom and top melting in all simulations performed. All Winton and Semtner-unlimited simulations with sea-ice cover larger than zero (i.e., all simulations except 5000 ppmv started from ice-free conditions) are investigated. The annual mean of heat flux for top (a) and bottom (b) melting averaged over the ice-cover are calculated and plotted against the annual global mean surface temperature in Figure 6.7.

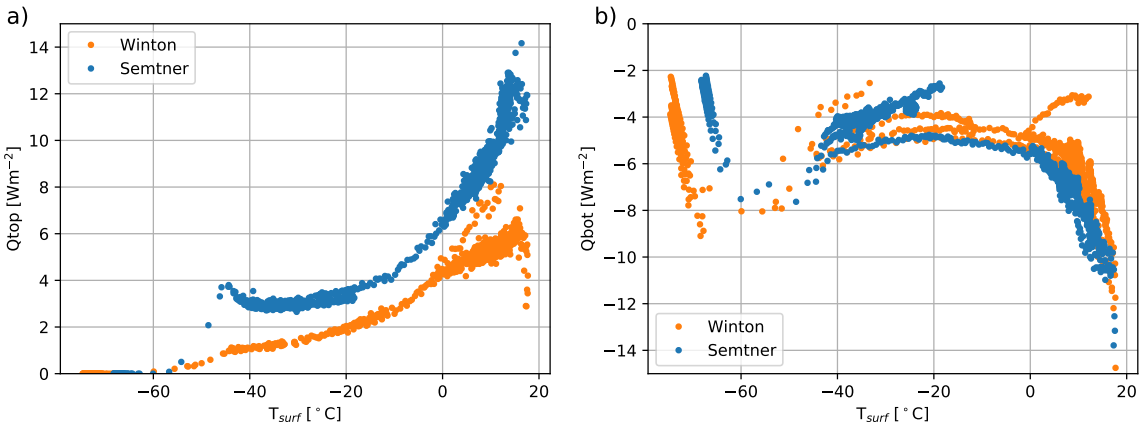


Figure 6.7: a) Annual mean heat flux available for top melting averaged over the sea-ice cover against the global average surface temperature and b) annual-mean heat flux available for bottom melting averaged over the sea-ice cover against the global average surface temperature. All Winton and Semtner-unlimited simulations with sea-ice cover larger than 0 are included.

It is worth noting that the sum of bottom and top global heat fluxes depicted in Figure 6.7 is bigger than $0\,\mathrm{W\,m^{-2}}$. However, this does not indicate that the ice is melting in total, because the heat flux is not the only quantity that governs ice growth, there is also precipitating snow. The snow that accumulates on top of the ice and melts during day or summer is also included in the surface heat flux. Because of this, the surface heat flux shows more melting than the bottom heat flux shows freezing, even tough the amount of ice is growing in total.

The same effect on top melting that has been shown at the ice edge in the previous section is visible in the global mean in Figure 6.7 a). Given the same global-mean surface temperature, the resulting heat flux for top melting is smaller in the Winton model than in the Semtner model, meaning that the Winton model melts less ice. This difference is especially notable at temperatures above the melting point, where it reaches values up to $\sim 6\,\mathrm{W\,m^{-2}}$ for the Winton model, whereas the Semtner model shows a heat flux higher than $12\,\mathrm{W\,m^{-2}}$. With decreasing temperatures, both the heat flux and the difference between them decreases, which can be explained by the fact that melting only takes place at an increasingly smaller fraction of the growing sea-ice cover. However, the Semtner model always causes melting greater than the Winton model by a factor of 1.5 to 2. This difference vanishes when both models reach $0\,\mathrm{W\,m^{-2}}$ top melting when global-mean temperatures fall below $-60\,°\mathrm{C}$, as surface melting stops almost completely on a Snowball Earth.

In Figure 6.7 b), the bottom heat flux shows much smaller differences between the Winton model and the Semtner model. Generally, the Semtner model causes a heat flux that is greater than the heat flux caused by the Winton model (i.e., the Semtner model causes more ice growth). However, there is a larger fluctuation between the individual simulations using each the Winton model and the Semtner model, especially if the global sea-ice cover is retreating. This can be attributed to the growing ice thickness, which weakens the bottom growth both in the Semtner model and the Winton model, in addition to the heat capacity that further weakens the bottom growth in the Winton model.

Summarizing the effects of increased vertical ice resolution on global-mean ice growth, using the 3-layer Winton model instead of the 0-layer Semtner model results in decreased top melting and increased bottom melting. Due to the fact that the decrease of top melting is larger, net melting

is decreased. This results in a weakening of the melt-ratchet effect, which takes place both on a diurnal and annual scale, and leads to decreased ice melt and therefore increased ice growth. The result is that the sea-ice cover of the Winton model can grow in simulations that are warmer due to a higher $CO_2$ content in comparison to the Semtner simulations. Therefore, the ice-albedo feedback is enhanced and the bifurcation diagram is changed as described in Section 6.2.1.

### 6.2.5 Effects on Reflected Shortwave Radiation

The global decrease of surface melting using the Winton model also impacts the surface albedo of ice. Using the ICON model in an aquaplanet setup, the surface albedo exhibits values in one of three regimes depending on the presence of sea ice and snow as depicted in Figure 6.8. The lowest surface albedo is for open ocean, which increases if sea ice forms or snow accumulates on the ice. Additionally, if the surface temperature of ice or snow exceeds $-1\,°C$, the albedo is starting to be linearly decreased down to a value for wet ice or snow when the surface temperature reaches $0\,°C$. The surface albedo is thus strongly influenced by the surface temperature and surface melting. The higher surface melting of the Semtner model shown in Section 6.2.4 impacts the surface albedo in multiple ways. The biggest effect takes place if total melting of ice occurs, replacing high snow or ice albedo by low ocean albedo. Due to the higher melting rates caused by the Semtner model in comparison to the Winton model, this is more likely to happen if the Semtner model is applied. This decrease in albedo would further heat up the local surface temperatures in the Semtner model and thus lead to additional melting in the vicinity, while the Winton model still shows higher surface albedo and less melting. This is the same effect as described by Abbot et al. (2010), where a decreased number of ice layers led to increased surface melting and thus faster removal of the ice, which resulted in faster global deglaciation.

The same change in surface albedo can occur even if there is still sea ice. Higher surface melting in the Semtner model can remove the snow cover and expose the darker ice surface, while the Winton model still has brighter snow present. Additionally, even if no surface melting occurs, a change in surface albedo can happen if the Semtner model shows a warmer surface temperature, which darkens the albedo due to the occurrence of warm ice or snow.

A further influence is the phase difference of ice thickness and sea-ice cover that is introduced when a higher vertical resolution is used (Semtner (1984), cf. Section 2.3). Due to the added heat capacity, the date of maximum ice extent is moved back into the spring and summer. The higher incoming solar radiation during these months increases the cooling effect of the sea-ice cover by increasing reflected shortwave radiation. So even if the mean sea-ice cover is the same, the reflected shortwave radiation can still be different.

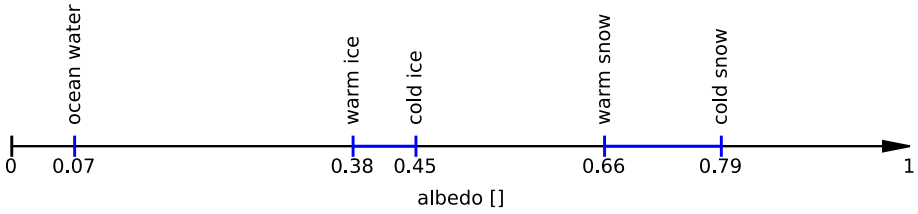


Figure 6.8: Surface albedo of all surface types in the ICON model setup.

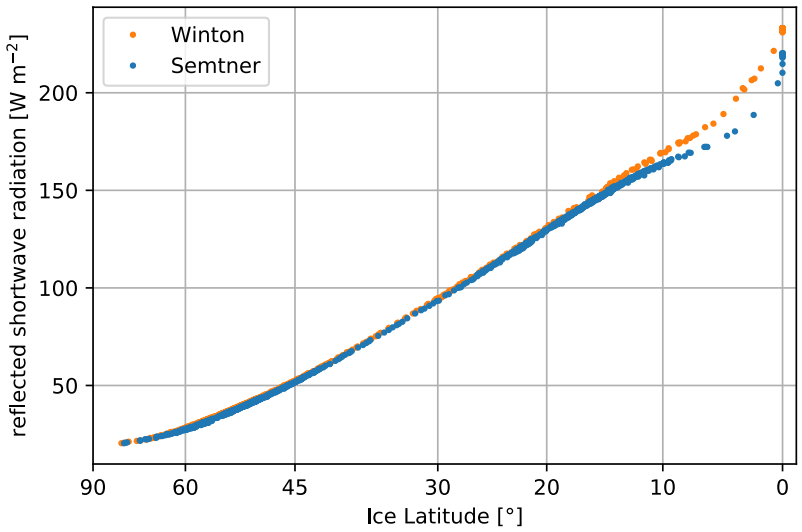


Figure 6.9: Global annual mean clear sky shortwave radiation reflected from the surface in dependency of the ice latitude. All Winton and Semtner-unlimited simulations with sea-ice cover larger than 0 are included.

The global impact of this change in surface albedo is shown by depicting the global-mean shortwave radiation that is reflected from the surface in Figure 6.9. It is apparent that for the same ice latitude, the Winton model reflects more shortwave radiation than the Semtner model. When ice is only present near the poles, the difference is marginal, which can be explained by the fact that ice at higher latitudes has a smaller impact on global-mean albedo. However, if the ice latitude exceeds $\sim 15°$, the difference increases. When a global sea-ice cover is reached, the Winton model reflects $\sim 13\,\mathrm{W\,m^{-2}}$ more shortwave radiation globally. This is due to the fact that in the Winton model, the whole Earth is covered in snow colder than $-1°$. The Semtner model on the other hand still shows surface melting in the tropics, resulting in the existence of bare sea ice for a period of time. The resulting decrease in albedo leads to the decreased reflected shortwave radiation.

In summary, it can be said that the increased surface melting in the Semtner model increases the global-mean albedo. Firstly, more melting shrinks the sea-ice cover, decreasing the global-mean albedo. Secondly, the albedo of the sea ice itself is decreased by increased surface melting and therefore less snow and warmer ice and snow.

### 6.2.6 Impact on the Jormungand State

The influence of increased vertical sea-ice resolution on the Jormungand cannot be determined using the simulations performed in this thesis, as no stable Jormungand state has been found. However, an assessment can be made due to the demonstrated impact of increased vertical sea-ice resolution on the initiation of Snowball Earth.

Section 6.2.5 shows that the Winton model results in a higher global albedo due to colder daily maximum temperatures and thus generally higher sea-ice albedo and more sea ice . The Jormungand state is stabilized by the albedo difference between snow-covered and bare sea ice (Abbot et al., 2011). This difference is expected to decrease, because colder surface temperatures using

the Winton model allow snow to accumulate in regions where it would have melted at warmer surface temperatures. This eliminates the albedo difference at this grid point. Increasing the vertical resolution of sea ice is thus expected to destabilize the Jormungand state by some extend, due to an increased ice-albedo feedback and consequential decreased albedo contrast of sea-ice in the tropics.

## 6.3 Summary

In this chapter, the impact of different sea-ice schemes using 0 layers (Semtner model) or 3 layers (Winton model) on Snowball Earth has been investigated. The results obtained can be summarised as follows.
The Winton model predicts internal ice temperatures and thus considers the heat capacity of the ice layers (Section 4.1.2), in contrast to the Semtner model. The heat capacity most importantly dampens the diurnal cycle of surface temperature, which consequently decreases top melting (Section 6.2.4) due to lower maximum surface temperatures. The diurnal cycle shows these effects both using an idealized setup of the Semtner and Winton model with artificial boundary conditions (Section 6.2.2), as well as in investigations of the ice edge in ICON with high-frequency model output (Section 6.2.4). This results in two effects on the global scale:

- Faster ice growth due to less efficient melting (Section 6.2.4).
- Higher surface albedo due to lower maximum surface temperatures (Section 6.2.5).

Both of these effects enhance the ice-albedo feedback on a global scale and in consequence amplify Snowball Earth initiation. Using the Winton model thus leads to global glaciation at higher atmospheric $CO_2$ contents. In the bifurcation diagram in Section 6.2.1 this becomes especially visible, as the bifurcation point in the Winton simulations is located at a $CO_2$ content $\sim 800\,\text{ppmv}$ or 52% higher than in the Semtner simulations.
A potentially existing hidden Jormungand state would thus also need a higher $CO_2$ content to be stable. Additionally, the stronger ice-albedo feedback is expected to destabilize the Jormungand state.

## 6.4 Discussion

The results of this chapter are in agreement to the findings of Abbot et al. (2010). There, it is concluded that using a sea-ice scheme with a low vertical resolution may hugely overestimate the surface temperature cycle in a Snowball climate, resulting in an underestimation of $CO_2$ required for deglaciation. In this thesis, a 0-layer and a 3-layer sea-ice model are compared instead of the 2, 4 and 60-layer sea-ice models used by Abbot et al. (2010). Additionally, glaciation is investigated in this thesis instead of deglaciation. The results are consistent, however: the lower vertical resolution increases the diurnal cycle of surface temperature, resulting in more efficient surface melting and an underestimation of $CO_2$ required for glaciation. Bottom freezing is also increased by reducing the vertical resolution; however, this is not enough to compensate for the much larger effect on surface melting.

Additionally, an effect related to the increased surface melting has been shown: the decrease of surface albedo for sea-ice models with lower vertical resolution. Both effects are interlinked, as surface melting affects surface albedo and vice versa, so the magnitude of each effect alone cannot be assessed without further investigations.
In total, this results in an increase in $CO_2$ at the glaciation bifurcation point by a factor of 1.5, for increasing the vertical resolution of ice from 0 to 3. Yang et al. (2012) showed that increasing the albedo of ice by 0.05 increases the $CO_2$ content at the bifurcation point by a factor of 2, and introducing sea-ice dynamics increases the $CO_2$ by a factor of 100 according to Voigt and Abbot (2012). So while the impact of the ice vertical resolution is small in comparison to the impact of ice dynamics, it still is a large factor if thermodynamical ice schemes are considered.
Especially the change in surface albedo gains more importance the further the ice reaches towards the equator. This could potentially affect the stability of near-snowball states such as the Jormungand state.

# 7 Conclusion

In this thesis, the impact of a sea-ice thickness limit and different vertical resolutions of sea ice on the initiation of Snowball Earth were tested. Limiting sea-ice thickness to 5 m results in an artificial heat flux from the ocean into the atmosphere, due to the large temperature differences between atmosphere and ocean, separated only by a thin layer of ice. This heats up the atmosphere in such a way that the atmospheric $CO_2$ content required for Snowball Earth is decreased by 5%. This artificial heat flux increases with growing sea-ice cover and falling temperatures, resulting in a heating of the atmosphere that corresponds to a reduction of $CO_2$ by a factor of 0.33 when a Snowball Earth is reached.

The sea-ice thickness limit is originally implemented to allow for the representation of ocean currents. These ocean currents have a significantly stronger impact on the Snowball Earth bifurcation than the associated thickness limit (Poulsen and Jacob, 2004). If no such thickness limit is required, for example due to the use of a mixed layer ocean, the impact of the artificial heating should be avoided by allowing for an unlimited ice thickness, especially if states with a large sea-ice cover are considered.

Increasing the vertical resolution from zero to three layers adds a heat capacity to the sea ice, which dampens the diurnal cycle of surface temperatures. This weakens the melt-ratchet effect, resulting in less efficient surface melting. Additionally, the reduced surface melting increases the surface albedo of the sea ice by allowing snow to be present on the ice for a longer time as well as decreasing the maximum surface temperatures. In total, this leads to easier Snowball Earth initiation. The draw-down of atmospheric $CO_2$ required for global glaciation to start is reduced and the level of atmospheric $CO_2$ at which Snowball Earth initiation occurs is increased by 50%, or a factor of 1.5. Compared to the impact of sea-ice dynamics, which increased the maximum $CO_2$ content by a factor of 100 (Voigt and Abbot, 2012), this influence is small. However, if thermodynamic sea-ice schemes are considered, the vertical resolution gains in importance. For example, increasing the surface albedo of sea ice by 0.05 leads to an increase of $CO_2$ for initiation of the same magnitude, by a factor of 2 (Yang et al., 2012).

The findings of Abbot et al. (2010) are complemented in this thesis by showing that increasing vertical ice resolution enhances Snowball Earth initiation by the same means by which it impedes Snowball Earth termination. The importance of a higher vertical resolution of thermodynamic sea-ice schemes in simulations of Snowball Earth is thus further emphasized. This is particularly important when accurate estimations of the position of the bifurcation points for Snowball initiation or termination are to be made. Additionally, it is likely that increasing vertical resolution destabilizes other Snowball states like the Jormungand state, as snow can accumulate easier on the ice. However, further research is required to investigate this influence.

The results of this thesis could be further extended in two ways. Firstly, by performing ICON simulations with higher temporal and spatial output resolution. This would allow for a more detailed

investigation of the sea-ice surface effects at the ice edge at different latitudes. By doing this, the melt-ratchet effect and its dependence on the different sea-ice resolutions could be investigated in different climate states (e.g., in a Jormungand state).
Secondly, by extending the investigation of sea-ice physics using offline sea-ice schemes with idealized boundary conditions. By defining a distinct set of boundary conditions corresponding to certain latitudes in certain climate states, one could show the sensitivity of the ice layer to different boundary conditions for different vertical resolution. On the one hand, this would allow for a more quantitative comparison with the results of Abbot et al. (2010), on the other hand it could reveal possibilities of tuning the sea-ice schemes to reduce the influence of vertical sea-ice resolution (e.g by refining the vertical sea-ice resolution near the ice-atmosphere surface as proposed by Abbot et al. (2010)).

# Bibliography


Abbot, D. S., I. Eisenman, and R. T. Pierrehumbert, 2010: The Importance of Ice Vertical Resolution for Snowball Climate and Deglaciation. *Journal of Climate*, **23 (22)**, 6100–6109.

Abbot, D. S., A. Voigt, M. Branson, R. T. Pierrehumbert, D. Pollard, G. L. Hir, and D. D. B. Koll, 2012: Clouds and Snowball Earth deglaciation. *Geophysical Research Letters*, **39 (20)**.

Abbot, D. S., A. Voigt, and D. Koll, 2011: The Jormungand global climate state and implications for Neoproterozoic glaciations. *Journal of Geophysical Research*, **116 (D18103)**.

Bitz, C. M. and W. H. Lipscomb, 1999: An energy-conserving thermodynamic model of sea ice. *Journal of Geophysical Research: Oceans*, **104 (C7)**, 15 669–15 677.

Budyko, M. I., 1969: The effect of solar radiation variations on the climate of the Earth. *Tellus*, **21 (5)**, 611–619.

Curry, J. A., J. L. Schramm, and E. E. Ebert, 1995: Sea Ice-Albedo Climate Feedback Mechanism. *J. Climate*, **8 (2)**, 240–247.

Donnadieu, Y., Y. Goddéris, G. Ramstein, A. Nédélec, and J. Meert, 2004: A 'snowball Earth' climate triggered by continental break-up through changes in runoff. *Nature*, **428 (6980)**, 303–306.

Giorgetta, M. A., R. Brokopf, T. Crueger, M. Esch, S. Fiedler, J. Helmert, C. Hohenegger, L. Kornblueh, M. Köhler, E. Manzini, T. Mauritsen, C. Nam, T. Raddatz, S. Rast, D. Reinert, M. Sakradzija, H. Schmidt, R. Schneck, R. Schnur, L. Silvers, H. Wan, G. Zängl, and B. Stevens, 2018: ICON-A, the Atmosphere Component of the ICON Earth System Model: I. Model Description. *Journal of Advances in Modeling Earth Systems*, **10 (7)**, 1613–1637.

Hoffman, P. F., 2009: Pan-glacial—a third state in the climate system. *Geology Today*, **25 (3)**, 100–107.

Hoffman, P. F., D. S. Abbot, Y. Ashkenazy, D. I. Benn, J. J. Brocks, P. A. Cohen, G. M. Cox, J. R. Creveling, Y. Donnadieu, D. H. Erwin, I. J. Fairchild, D. Ferreira, J. C. Goodman, G. P. Halverson, M. F. Jansen, G. L. Hir, G. D. Love, F. A. Macdonald, A. C. Maloof, C. A. Partin, G. Ramstein, B. E. J. Rose, C. V. Rose, P. M. Sadler, E. Tziperman, A. Voigt, and S. G. Warren, 2017: Snowball Earth climate dynamics and Cryogenian geology-geobiology. *Science Advances*, **3 (11)**, e1600 983.

Kirschvink, J. L., 1992: Late Proterozoic Low-Latitude Global Glaciation: the Snowball Earth. *The Proterozoic Biosphere: A Multidisciplinary Study*, Schopf, J. W. and C. Klein, Eds. (Cambridge University Press, New York, 1992), 51–52.

Lewis, J. P., A. J. Weaver, and M. Eby, 2006: Deglaciating the snowball Earth: Sensitivity to surface albedo. *Geophysical Research Letters*, **33 (23)**.

Maykut, G. A. and N. Untersteiner, 1969: *Numerical prediction of the thermodynamic response of Arctic sea ice to environmental changes* (The Rand Corporation, Santa Monica, California, 1969).

———, 1971: Some results from a time-dependent thermodynamic model of sea ice. *Journal of Geophysical Research (1896-1977)*, **76 (6)**, 1550–1575.

Mitra, A. and I. M. L. Das, 2007: Simulation of Antarctic sea ice. *Current Science*, **92 (3)**, 345–350.

Myhre, G., E. J. Highwood, K. P. Shine, and F. Stordal, 1998: New estimates of radiative forcing due to well mixed greenhouse gases. *Geophysical Research Letters*, **25 (14)**, 2715–2718.

Notz, D. and C. Bitz, 2016: Sea ice in Earth system models. *Sea Ice*, Thomas, D. N., Ed. (John Wiley & Sons, Ltd, 2016), 3d ed., 304–325.

Pierrehumbert, R. T., D. S. Abbot, A. Voigt, and D. Koll, 2011: Climate of the Neoproterozoic. *Annual Review of Earth and Planetary Sciences*, **39 (1)**, 417–460.

Poulsen, C. J. and R. L. Jacob, 2004: Factors that inhibit snowball Earth simulation. *Paleoceanography and Paleoclimatology*, **19 (4)**.

Runnegar, B., 2000: Loophole for snowball Earth. *Nature*, **405 (6785)**, 403–404.

Schrag, D. P. and P. F. Hoffman, 2001: Life, geology and snowball Earth. *Nature*, **409 (6818)**, 306–306.

Sellers, W. D., 1969: A Global Climatic Model Based on the Energy Balance of the Earth-Atmosphere System. *J. Appl. Meteor.*, **8 (3)**, 392–400.

Semtner, A. J., 1976: A Model for the Thermodynamic Growth of Sea Ice in Numerical Investigations of Climate. *Journal of Physical Oceanography*, **6 (3)**, 379–389.

———, 1984: On modelling the seasonal thermodynamic cycle of sea ice in studies of climatic change. *Climatic Change*, **6 (1)**, 27–37.

Stevens, B., M. Giorgetta, M. Esch, T. Mauritsen, T. Crueger, S. Rast, M. Salzmann, H. Schmidt, J. Bader, K. Block, R. Brokopf, I. Fast, S. Kinne, L. Kornblueh, U. Lohmann, R. Pincus, T. Reichler, and E. Roeckner, 2013: Atmospheric component of the MPI-M Earth System Model: ECHAM6. *Journal of Advances in Modeling Earth Systems*, **5 (2)**, 146–172.

Voigt, A. and D. S. Abbot, 2012: Sea-ice dynamics strongly promote Snowball Earth initiation and destabilize tropical sea-ice margins. *Clim. Past*, **8 (6)**, 2079–2092.

Voigt, A., D. S. Abbot, R. T. Pierrehumbert, and J. Marotzke, 2011: Initiation of a Marnoun Snowball Earth in a state-of-the-art atmosphere-ocean general circulation model. *Climate of the Past*, **7**, 249–263.

Warren, S. G., R. E. Brandt, T. C. Grenfell, and C. P. McKay, 2002: Snowball Earth: Ice thickness on the tropical ocean. *Journal of Geophysical Research: Oceans*, **107 (C10)**, 3167.

Winton, M., 2000: A Reformulated Three-Layer Sea Ice Model. *J. Atmos. Oceanic Technol.*, **17 (4)**, 525–531.

Yang, J., W. R. Peltier, and Y. Hu, 2012: The Initiation of Modern "Soft Snowball" and "Hard Snowball" Climates in CCSM3. Part I: The Influences of Solar Luminosity, $CO_2$ Concentration, and the Sea Ice/Snow Albedo Parameterization. *J. Climate*, **25 (8)**, 2711–2736.

# Acknowledgement

First of all, I would like to thank Christoph Braun for his mentoring, patient explanations and encouragement. His guidance enabled me to do my best. I would like to express my deepest gratitude to Dr. Aiko Voigt for the excellent supervision and extensive feedback. I am grateful to Prof. Joaquim Pinto for taking the role of second advisor and his constructive feedback. I would also like to thank all members of the working group Clouds and Storm Tracks for their assistance in person as well as in home office.

I'm extremely grateful to my friends and family for their continuous support and encouragement through all the ups and downs of the last year. Thanks to Freia for proofreading and putting structure in my thought process. Finally, special thanks to Natalija for the essential support in writing this thesis during quarantine.

# Erklärung

Ich versichere wahrheitsgemäß, die Arbeit selbstständig angefertigt, alle benutzten Hilfsmittel vollständig und genau angegeben und alles kenntlich gemacht zu haben, was aus Arbeiten anderer unverändert oder mit Abänderungen entnommen wurde.

Karlsruhe, den 14.08.2020

Johannes Hörner